FoxO transcription factors are required for hepatic HDL-cholesterol clearance

Samuel X. Lee, … , Franz Rinninger, Rebecca A. Haeusler

Research Article   In-Press Preview   Metabolism

Insulin resistance and type 2 diabetes are associated with low levels of high-density lipoprotein-cholesterol (HDL-C). The insulin-repressible FoxO transcription factors are potential mediators of insulin's effect on HDL-C. FoxOs mediate a substantial portion of insulin-regulated transcription, and poor FoxO repression is thought to contribute to the excessive glucose production in diabetes. In this work, we show that mice with liver-specific triple FoxO knockout (L-FoxO1,3,4), which are known to have reduced hepatic glucose production, also have increased HDL-C. This was associated with decreased expression of HDL-C clearance factors, scavenger receptor class B type I (SR-BI) and hepatic lipase, and defective selective uptake of HDL-cholesteryl ester by the liver. The phenotype could be rescued by re-expression of SR-BI. These findings demonstrate that hepatic FoxOs are required for cholesterol homeostasis and HDL-mediated reverse cholesterol transport to the liver.

Find the latest version:

FoxO Transcription Factors are Required for Hepatic HDL-Cholesterol Clearance

Samuel X. Lee[1#], Markus Heine[2#], Christian Schlein[2], Rajasekhar Ramakrishnan[3], Jing Liu[3], Gabriella Belnavis[1], Ido Haimi[1], Alexander W. Fischer[2], Henry Ginsberg[3], Joerg Heeren[2], Franz Rinninger[2,4*], and Rebecca A. Haeusler[1,5*]

[1] Naomi Berrie Diabetes Center, Columbia University College of Physicians and Surgeons, New York NY
[2] Department of Biochemistry and Molecular Cell Biology, University Medical Center Hamburg Eppendorf, 20246 Hamburg, Germany
[3] Department of Medicine, Columbia University College of Physicians and Surgeons, New York NY
[4] Department of Internal Medicine III, University Medical Center Hamburg Eppendorf, 20246 Hamburg, Germany
[5] Department of Pathology and Cell Biology, Columbia University College of Physicians and Surgeons, New York NY

[#] these authors contributed equally to this work

*The authors have declared that no conflict of interest exists

*Contact:
Rebecca A. Haeusler
1150 Saint Nicholas Ave, Room 303A, New York NY 10032 USA
+1 (212) 851-4899
rah2130@columbia.edu

and

Franz Rinninger
University Medical Center Eppendorf, Martinistrasse 52, Hamburg 20146 Germany
49 / 40 / 7410 5 2905
rinninger@uke.de

Abstract

Insulin resistance and type 2 diabetes are associated with low levels of high-density lipoprotein-cholesterol (HDL-C). The insulin-repressible FoxO transcription factors are potential mediators of insulin's effect on HDL-C. FoxOs mediate a substantial portion of insulin-regulated transcription, and poor FoxO repression is thought to contribute to the excessive glucose production in diabetes. In this work, we show that mice with liver-specific triple FoxO knockout (L-FoxO1,3,4), which are known to have reduced hepatic glucose production, also have increased HDL-C. This was associated with decreased expression of HDL-C clearance factors, scavenger receptor class B type I (SR-BI) and hepatic lipase, and defective selective uptake of HDL-cholesteryl ester by the liver. The phenotype could be rescued by re-expression of SR-BI. These findings demonstrate that hepatic FoxOs are required for cholesterol homeostasis and HDL-mediated reverse cholesterol transport to the liver.

Introduction

The liver is a critical site for maintaining metabolic homeostasis. In hepatocytes, the forkhead transcription factors of the FoxO sub-family, FoxO1, FoxO3, and FoxO4 (FoxOs), mediate a substantial portion of insulin-regulated gene transcription (1-5). During fasting, FoxOs are active, whereas insulin signaling suppresses FoxO activity via Akt-mediated phosphorylation and nuclear exclusion (6, 7). The three FoxOs work in concert to promote expression of their target genes (8). Previously, we have demonstrated that liver-specific ablation of these three hepatic FoxOs in mice prevents the induction of glucose-6-phosphatase and the repression of glucokinase during fasting, thereby increasing lipogenesis at the expense of glucose production (9). FoxOs are also required for expression of multiple other genes involved in liver metabolic pathways (10-12). These findings demonstrate that hepatic FoxOs play a vital role in maintaining proper glucose and lipid homeostasis.

The liver also plays an essential role in cholesterol metabolism. One important aspect is to facilitate the clearance of cholesterol from circulating high-density lipoprotein (HDL) particles into the liver, where it can be converted to bile acids or transported directly into the bile to be excreted in the feces (13, 14). HDL-cholesterol (HDL-C) is primarily cleared by scavenger receptor class B type I (SR-BI), a liver membrane receptor that

mediates selective HDL-cholesteryl ester (CE) uptake, defined as lipid internalization independent of holo-particle uptake (15, 16). Acting alongside SR-BI is the enzyme, hepatic lipase (HL) (17). Studies show that (i) HL is a liver-secreted enzyme that hydrolyzes triglycerides and phospholipids, and is involved in processing large lipid-rich HDL to smaller HDL (18), and (ii) HL's ligand-binding activity may mediate interactions of lipoproteins with SR-BI or the plasma membrane, thus facilitating selective HDL-CE uptake (19-24). As such, mice lacking expression of either SR-BI or HL have elevated levels of HDL-C and impaired HDL-C clearance by hepatocytes (14, 25-28).

In the current study, we utilized mice with liver-specific ablation of three hepatic FoxOs (L-FoxO1,3,4) (8, 9) and littermate controls with the genotype $Foxo1^{flox/flox}$, $Foxo3^{flox/flox}$, and $Foxo4^{flox/Y}$, to explore the role of hepatic FoxOs in regulating HDL-C metabolism. We observed that L-FoxO1,3,4 mice have an increase in plasma HDL-C, especially when challenged with a western-type diet (WTD). Moreover, we also found that hepatic FoxOs are required for the expression of HDL-C clearance factors, SR-BI and HL, suggesting that selective HDL-CE uptake by the liver may be diminished in L-FoxO1,3,4 mice. In order to directly measure selective HDL-CE clearance, metabolic studies were performed using HDL that was radiolabeled in both the protein (^{125}I) and the lipid ($[^{3}$H]) moieties. We found that selective HDL-CE uptake by the liver was reduced in L-FoxO1,3,4 mice

in vivo as well as in isolated L-FoxO1,3,4 primary murine hepatocytes *in vitro*. Moreover, the accumulation of HDL-C in L-FoxO1,3,4 mice was attenuated by rescue of SR-BI expression. Thus, our data indicate that the increase in plasma HDL-C in L-FoxO1,3,4 mice is primarily a consequence of reduced HDL lipid uptake by the liver. These findings suggest that, in addition to the established effects on glucose and triglyceride metabolism, hepatic FoxOs are required for HDL-mediated reverse cholesterol transport, a key mechanism of lipid homeostasis *in vivo*.

Results

Deletion of Hepatic FoxOs Increases Cholesterol Accumulation in Large HDL Particles.

We first measured plasma cholesterol in chow-fed mice, and found 50% higher plasma cholesterol in L-FoxO1,3,4 mice compared to littermate controls (**Figure 1A**). In order to determine the distribution of cholesterol with respect to lipoprotein fractions, we separated the plasma by fast protein liquid chromatography (FPLC). We found that chow-fed L-FoxO1,3,4 mice had increased HDL-C and accumulation of cholesterol in the fractions that elute similarly to large HDL (**Figure 1B**). We performed western blot analysis of these fractions and found that apoA-I, the major apolipoprotein of HDL, is shifted to the left, indicating larger HDL particles. We also found a leftward shift of apoE (**Figure 1C**), which is consistent with the well-established characteristics of large, spherical HDL particles (29, 30). In contrast, apoB-containing particles eluted much earlier, peaking at fraction 46-48 (not shown) and disappearing by fraction 52, indicating that there is little to no difference in LDL-C between genotypes. There were no differences in total plasma apoA-I (**Supplemental Figure S1A**), suggesting that the leftward shift of apoA-I, apoE, and HDL-C indicates the presence of larger HDL particles in L-FoxO1,3,4 mice.

Next, we challenged the mice with a western-type diet (WTD) consisting of 21% milkfat and 0.2% cholesterol. The WTD is known to increase plasma cholesterol levels and to induce atherogenesis in susceptible strains (31). After three weeks of WTD feeding, L-FoxO1,3,4 mice showed 65% higher plasma cholesterol compared to WTD-fed controls (**Figure 1D**). The cholesterol profile in the knockouts was exacerbated on this diet, showing accumulation of cholesterol in fractions that elute similarly to large HDL (**Figure 1E**). Consistent with this, there was a leftward shift in apoA-I (**Figure 1F**). There was also abundant accumulation of apoE in these shifted fractions, similar to what is seen in other experimental mouse models with elevated HDL levels (14, 32). On WTD, there were no differences in total plasma apoA-I (**Supplemental Figure S1B**). These data support the hypothesis that hepatic FoxOs play a role in HDL-C metabolism.

FoxOs are Required for Expression of Scavenger Receptor SR-BI and Hepatic Lipase

To identify contributors to the accumulation of plasma HDL-C in L-FoxO1,3,4 mice, we queried microarrays from livers of L-FoxO1,3,4 mice (9) for genes involved in HDL synthesis and clearance (**Supplemental Table S1**). We found no differences in genes regulating HDL synthesis or biliary excretion, including *Abca1, Apoa1, Apoa2, Lcat, Apoe*, *Abcg5,* and *Abcg8*. We also found no significant differences in *Apoc3*, *Srebp2, Hmgcr,* or *Pltp.* However,

L-FoxO1,3,4 mice showed reduced expression of two genes involved in HDL-C clearance: *Scarb1* (which encodes SR-BI) and *Lipc* (which encodes HL). Using quantitative PCR, we verified that L-FoxO1,3,4 mice showed significant reductions in *Scarb1* and *Lipc* during both chow and WTD feeding (**Figure 2A-B**). We also verified that there were no differences in *Abca1, Apoa1, Apoa2, Apoc3, Apoe, Lcat, Srebp2, Hmgcr, Abcg5,* or *Abcg8*. By qPCR, there was an increase in *Pltp* expression, however increased Pltp alone is insufficient to increase HDL-C (33). These data suggest that the increase in plasma HDL-C in L-FoxO1,3,4 mice is due to defective clearance.

We next confirmed that these decreases in *Scarb1* and *Lipc* mRNA result in decreases at the protein level. By western blot, we found that in both chow-fed and WTD-fed mice, SR-BI protein levels decreased significantly (>85%) in liver lysates isolated from L-FoxO1,3,4 mice compared to those of control mice (**Figure 2C**). Consistent with what was observed from the gene expression data, we found no changes in liver ABCA1 protein levels between L-FoxO1,3,4 and control mice fed either chow or WTD (**Supplemental Figure S2**). To investigate HL, we measured its activity in non-heparinized plasma (34, 35). Compared to controls, L-FoxO1,3,4 mice had a 50% decrease in HL activity (**Figure 2C**). Taken together, these data demonstrate that hepatic FoxOs are required for normal expression of both SR-BI and HL.

HDL Metabolism in L-FoxO1,3,4 and Control Mice

To address HDL metabolism in more detail, we investigated the turnover of ^{125}I-TC-/[^{3}H]CEt-WT-HDL in control and L-FoxO1,3,4 mice on chow (**Figures 3-4**) and WTD (**Supplemental Figure S3-4**). We injected this murine HDL preparation intravenously in mice, and thereafter, we harvested blood samples during a 24-hour interval (15). In these studies, [^{3}H]CEt traces the clearance of HDL-associated CE, and ^{125}I-TC traces the clearance of HDL holo-particles (36). The difference between both tracers ([^{3}H]CEt - ^{125}I-TC) represents selective CE removal from HDL particles.

In control mice on chow, the plasma decay of HDL-associated [^{3}H]CEt was faster compared to ^{125}I-TC (**Figure 3A**), indicating selective CE removal from the HDL plasma pool by tissues. In L-FoxO1,3,4 mice on chow, the plasma decay of ^{125}I-TC was similar to control mice (**Figure 3B**). However, removal of HDL-associated [^{3}H]CEt from plasma was slower in L-FoxO1,3,4 mice compared to controls. Similarly, selective CE removal from the HDL plasma pool was also slower in WTD-fed L-FoxO1,3,4 mice compared to littermate controls (**Supplemental Figure S3A-B**). Thus, selective CE removal from HDL was significantly reduced in both chow-fed and WTD-fed L-FoxO1,3,4 mice. These results suggest that selective CE removal from the HDL plasma pool is substantially reduced in mice lacking hepatic FoxOs.

From decay curves shown in Figure 3A-B and Supplemental Figure S3A-B, we calculated the plasma-fractional catabolic rate (FCR) for both HDL-associated tracers on chow (**Figure 4A**) and WTD (**Supplemental Figure S4A**) (37). In control mice, the plasma-FCR for HDL-associated [^{3}H]CEt was substantially higher compared to ^{125}I-TC due to selective CE removal from plasma by tissues. In chow-fed L-FoxO1,3,4 mice, we detected no significant difference in plasma-FCR for ^{125}I-TC compared to control mice, although in WTD-fed L-FoxO1,3,4 mice, there was a slight decrease in ^{125}I-TC decay compared to littermate controls. However, on both diets, compared to controls, there was a significant reduction in plasma-FCR for [^{3}H]CEt, yielding a significantly reduced rate of selective CE removal from plasma in L-FoxO1,3,4 mice. This shows that there is reduced selective CE clearance from the plasma HDL pool by tissues in L-FoxO1,3,4 mice.

Next, we investigated HDL metabolism by defined organs. 24-hours after ^{125}I-TC-/[^{3}H]CEt-WT-HDL injection, we analyzed tracer content of tissues, and calculated HDL uptake in terms of organ-FCR (15). In control mice on both diets, the hepatic organ-FCR showed selective CE uptake by the liver from HDL (**Figure 4B and Supplemental Figure S4B**) that was in line with earlier studies in wild-type mice (26, 38). In L-FoxO1,3,4 mice on both diets, the hepatic uptake rate for ^{125}I-TC was similar to control mice. However, the hepatic organ-FCR for [^{3}H]CEt, and the selective CE uptake from HDL, were

decreased significantly compared to control mice on both diets. This indicates that hepatic selective uptake of HDL-CE is defective in L-FoxO1,3,4 mice.

Compared with the liver, the HDL tracer uptake rates were quantitatively low in all non-hepatic tissues. In adrenal glands, which also express SR-BI (16), chow-fed L-FoxO1,3,4 mice showed a trend towards reduced selective CE uptake (**Figure 4C**). However, this trend was not detected in WTD-fed L-FoxO1,3,4 mice (**Supplemental Figure S4C**). We did not expect SR-BI expression to be lower in L-FoxO1,3,4 adrenals, because this is a hepatocyte-specific FoxO knockout. Indeed, there was no change in both *Scarb1* and *Foxo1* gene expression in L-FoxO1,3,4 adrenals (**Supplemental Figure S5**). However, because HL is a secreted protein that is known to function in SR-BI–mediated uptake of HDL-C, we speculate that the low HL activity of L-FoxO1,3,4 mice could potentially contribute to the trend of lower selective CE uptake in other SR-BI–expressing tissues (such as adrenal gland), in chow-diet conditions. In the kidneys, which do not express SR-BI, organ-FCR's for both HDL-associated tracers did not differ between control and L-FoxO1,3,4 mice on either chow or WTD (**Figure 4D and Supplemental Figure S4D**). However, consistent with previous studies, kidney organ-FCRs for HDL-associated ^{125}I-TC were higher compared to HDL-associated [3H]CEt, which reflects a preferential renal catabolism of

HDL apolipoproteins (26). In spleen, stomach, intestine and carcass, the organ-FCR's for HDL-associated [^{3}H]CEt were decreased in chow-fed L-FoxO1,3,4 mice compared to controls (**Table 1**). Of these tissues, only the spleen showed selective uptake.

HDL Metabolism in Primary Murine Hepatocytes

Next, we investigated HDL-CE uptake into isolated primary hepatocytes from control and L-FoxO1,3,4 mice in a dose-response manner. Following a 4-hr seeding period, we incubated hepatocytes in medium containing ^{125}I-TC-/[^{3}H]CEt-WT-HDL at 10, 20, 40 or 100 µg HDL protein/ml for 2-hrs. In control hepatocytes, [^{3}H]CEt uptake is substantially higher than ^{125}I-TC at all doses, indicating selective CE uptake from HDL (**Figure 5A**). This observation is in line with previous results (26, 39). In L-FoxO1,3,4 hepatocytes, ^{125}I-TC uptake was similar to controls (**Figure 5B**). However, [^{3}H]CEt uptake was significantly decreased compared to control cells at all doses, yielding a ~50% decrease in selective CE uptake from HDL. We also measured HDL-CE uptake over a 2-hr time course at 20 µg HDL protein/ml (**Supplemental Figure S6A-B**). At all time points, selective HDL-CE uptake was significantly reduced by approximately 40 % in L-FoxO1,3,4 hepatocytes compared to controls. Western blot analysis confirmed that SR-BI protein levels are substantially decreased in L-FoxO1,3,4 hepatocytes compared to controls (**Figure 5C**). We also observed significantly lower

expression of *Scarb1* and *Lipc* mRNA from L-FoxO1,3,4 hepatocytes (**Figure 5D**). However, we noted that the mRNA of both genes declined over time after hepatocyte isolation, especially in wild-type hepatocytes, as was previously observed (40). Taken together, these experiments demonstrate that selective CE uptake from HDL is decreased in FoxO-deficient hepatocytes in a cell autonomous manner.

Rescuing SR-BI Reverses the Accumulation of HDL-C in L-FoxO1,3,4 mice

To determine whether SR-BI induction in the livers of FoxO-deficient mice can reverse the HDL-C phenotype, we transduced WTD-fed L-FoxO1,3,4 mice and littermate controls with an adenovirus expressing SR-BI (Ad.SR-BI). We titrated the virus to a low-dose to achieve only mild increases in SR-BI, because several-fold overexpression in wild-type mice is known to potently reduce HDL-C irrespective of the HDL subclass (13). Three days after virus injection, we measured SR-BI expression levels. As a result of the low titer we used, there were no increases in total SR-BI levels in control mice transduced with Ad.SR-BI compared to those transduced with a control virus (Ad.GFP) (**Figure 6A**). However, L-FoxO1,3,4 mice injected with Ad.SR-BI showed a five-fold increase in liver SR-BI compared to those injected with Ad.GFP. We noted that even after this five-fold increase, levels of SR-BI were still significantly lower than littermate control mice.

Transducing L-FoxO1,3,4 mice with SR-BI caused a substantial normalization of the HDL-C accumulation (**Figure 6B**). Western blots confirmed that the leftward shifts of apoA-I and apoE were also normalized (compare lanes 10-11 with lanes 4-5) (**Figure 6C**). Corresponding to the fact that the wild-type control mice transduced with this low-titer Ad.SR-BI showed no overexpression of SR-BI, there was no decrease of HDL-C in these mice. Neither *Lipc* mRNA expression nor plasma HL activity was affected by Ad.SR-BI transduction (**Supplemental Figure S7A-B**). Collectively, these findings demonstrate that rescuing SR-BI expression in hepatic FoxO-deficient mice is sufficient to reverse the accumulation of cholesterol in large HDL particles.

Acute depletion of hepatic FoxOs is sufficient to induce HDL phenotype

We predicted that *Scarb1* and *Lipc* are transcriptional targets of FoxOs, because (i) the mRNA expression of these genes is low in every condition tested, (ii) motif analysis using HOMER (41) identified dozens of FoxO consensus sequences in and near *Scarb1* and *Lipc* (**Supplemental Figure S8A-C**), and (iii) publicly available microarrays are consistent with this: transgenic overexpression of constitutively active FoxOs causes elevated liver expression of *Scarb1* mRNA (11). Moreover, mice lacking the insulin receptor substrate proteins (Irs1 and Irs2) – which are expected to have constitutively active FoxOs – have elevated liver expression of *Scarb1* and

reduced serum HDL-C. Importantly, concomitant knockout of FoxO1 with Irs1 and Irs2 partially normalizes this phenotype (5).

To further validate that decreases in *Scarb1* and *Lipc* are directly due to FoxO depletion, and not compensatory defects due to long-term genetic loss of FoxOs, we transduced chow-fed, adult *Foxo1^{flox/flox}*, *Foxo3^{flox/flox}*, and *Foxo4^{flox/Y}* control mice with an adeno-associated virus expressing Cre under a hepatocyte-specific promoter (AAV8.Tbg.Cre). Two weeks after the injection, we found that chow-fed triple-floxed mice transduced with AAV8.Tbg.Cre virus started to accumulate cholesterol in large HDL fractions (**Supplemental Figure S9**). Four weeks after virus injection, we euthanized the mice. At that time point, the HDL-C accumulation phenotype was exacerbated compared to the two–week time point (**Figure 7A**). We verified that AAV8.Tbg.Cre caused FoxO depletion, as well as low levels of *G6pc* and high levels of *Gck*, two known targets of FoxO transcriptional activation and repression, respectively (9) (**Figure 7B**). Moreover, it caused decreases in *Scarb1* and *Lipc* mRNA levels, as well as SR-BI protein levels (**Figure 7C**). The levels of *Scarb1* and *Lipc* mRNA were significantly correlated with the level of FoxO1 knockdown (**Figure 7D**).

Finally, we also measured protein expression levels of PDZK1 in L-FoxO1,3,4 liver lysates and primary hepatocytes. PDZK1 is a scaffold protein that is

essential for SR-BI stability and localization in hepatocytes, and has been reported to post-transcriptionally regulate SR-BI levels (42, 43). We found that in L-FoxO1,3,4 liver lysates and primary hepatocytes, there were no changes in PDZK1 expression levels between L-FoxO1,3,4 and matched controls. (**Supplemental Figure S10**). Thus we have no evidence for posttranslational regulation of SR-BI by FoxOs. Taken together, these data support a model whereby FoxOs acutely regulate Scarb1 and Lipc at the transcriptional level, thus impacting HDL-C levels and HDL-mediated reverse cholesterol transport.

Discussion

Here we report that hepatic FoxOs are required for normal hepatic clearance of HDL-C. Our results suggest that hepatic FoxOs promote the expression of SR-BI and HL, which induce HDL-C uptake from the plasma into the liver. This novel mechanism demonstrates the importance of these insulin-inactivated transcription factors in regulating HDL-C metabolism.

SR-BI and HL are both important for plasma HDL-C turnover. Both SR-BI and HL knockout mice have elevated plasma cholesterol levels and cholesterol accumulation in large HDL particles (14, 28) due to impaired selective uptake of HDL-CE by the liver (26, 27). Some studies have suggested that SR-BI and HL promote selective uptake by acting together

(44), although others indicate that the two act through independent mechanisms (24). Evidence in humans also shows important roles for SR-BI and HL in HDL-C metabolism. In genome-wide association studies, variants near both *Scarb1* and *Lipc* have been associated with HDL-C (45-47). Furthermore, individuals with HL deficiency were reported to have an accumulation of large, buoyant plasma HDL particles (48-50). Thus, mechanisms regulating HDL-C clearance through these two proteins may be relevant across species.

Hepatic FoxOs have also been shown to control other downstream aspects of hepatic cholesterol metabolism. Once HDL-CE enters the hepatocyte, it can be stored, secreted on lipoproteins, or excreted into the bile. There are two possible mechanisms to allow for cholesterol excretion into the bile. The first is to be secreted directly into the bile via the heterodimeric cholesterol transporters *Abcg5* and *Abcg8 (51, 52)*. The second is to be converted into bile acids through a series of enzymatic reactions, in which *Cyp7a1* encodes the rate-limiting enzyme (53, 54). All three genes – *Abcg5, Abcg8,* and *Cyp7a1* – are reportedly regulated by hepatic FoxO1 (55-58). Moreover, we have previously reported that an additional enzyme involved in bile acid synthesis, *Cyp8b1,* is a FoxO1 target (10). Our current findings that hepatic FoxOs also regulate clearance of HDL-C by the liver indicate that FoxOs have pleiotropic effects on hepatic cholesterol homeostasis.

The inactivation of hepatic FoxOs by insulin signaling has been well characterized (1, 59). Several experimental mouse models have shown that ablating the upstream FoxO regulators involved in this insulin signaling cascade (*e.g.* the insulin receptor, insulin receptor substrate proteins, or Akt) leads to impaired glucose homeostasis due to constitutive FoxO activation (4, 5, 60, 61). Thus, these models may also provide insight into the regulation of HDL-C levels via the insulin-FoxO pathway. For instance, liver ablation of the insulin receptor causes decreased serum HDL-C associated with a reduction in large, apoE containing HDL particles (60). Similarly, Irs1/2 double knockouts have elevated *Scarb1* mRNA and reduced serum HDL-C, whereas concomitant FoxO1 knockout of FoxO1 partially reverses this (5). Furthermore, transgenic overexpression of constitutively active FoxOs increases liver *Scarb1* mRNA (11). These data provide additional evidence to suggest that hepatic FoxOs directly mediate insulin's effect on HDL-C metabolism through their transcriptional effects on *Scarb1* and *Lipc.*

We propose that the regulation of HDL-C uptake by FoxOs is part of a larger program of hepatic insulin regulation of cholesterol metabolism. In addition to what is uncovered in the present work, liver insulin signaling is also known to positively regulate the Srebp2 pathway (60) and the levels of the

18

LDL receptor (62), and negatively regulate the catabolism of cholesterol into bile acids (63), biliary cholesterol excretion (55), and bile acid composition (10). It has been proposed that fatty acid and cholesterol metabolism are regulated by nutrient status in order to coordinate (i) the supply of cellular membrane components, and (ii) the usage of available precursor molecules (64). As insulin is a key regulator of the nutrient-rich state, it is possible that its actions coordinate glucose, fatty acid, *and* cholesterol flux to maintain overall energy homeostasis.

Given FoxOs' well-known role in promoting hepatic glucose production (65), our findings suggest a potential connection between plasma glucose and plasma HDL-C in the setting of type 2 diabetes. Patients with type 2 diabetes have elevated plasma glucose, along with reduced plasma HDL-C (66). As excessive FoxO activity is expected to contribute to high hepatic glucose production in these patients (65), perhaps it also contributes to their low HDL-C. Indeed, one of the FoxO targets we identified–HL–is known to have increased activity in type 2 diabetes patients (67, 68). Hence, it is possible that elevated FoxO activity in the setting of type 2 diabetes leads to more rapid HDL-C turnover.

It is of interest that L-FoxO1,3,4 mice accumulate cholesterol preferentially in large, apoE rich HDL particles, while the amount of cholesterol on

"traditional" sized HDL remains unchanged between genotypes. It has been reported that apoE facilitates the uptake of HDL-CE via SR-BI *in vivo* (69). Moreover, apoE-containing HDL may be a preferred substrate for HL (70, 71). Thus it is possible that these preferences of SR-BI and HL may contribute to the specific accumulation of apoE-containing HDL in L-FoxO1,3,4 mice. Another observation we noted was that the difference in HDL-C between genotypes was exacerbated on the WTD, despite the fact that HL is halved and SR-BI is exceedingly low in L-FoxO1,3,4 mice on both diets. What is the cause of this HDL-C exacerbation? Interestingly, SR-BI knockout mice also show the same exacerbation: differences in HDL-C between SR-BI knockout mice and controls are greater after western diet feeding than chow diet feeding (72). Thus the exacerbation is independent of additional SR-BI lowering. We speculate that multiple factors may be involved, including changes on the particles themselves. Some of these may include alterations in other HDL lipid species, or HDL-bound proteins, or potential increased competition for clearance of apoE-rich HDL particles via the alternative pathway of LDLR/LRP1/HSPGs (in other words, western-diet induced increases in apoB-containing particles may compete with apoE-rich HDL for binding to LDLR/LRP1/HSPG).

In this work, we have demonstrated a novel link between the insulin-repressible FoxO transcription factors and HDL-mediated reverse cholesterol

transport. This cardioprotective pathway is a critical step for the excretion of cholesterol from the periphery to the feces (73-76). Indeed, patients with a rare loss-of-function variant in the gene encoding SR-BI have significantly increased levels of plasma HDL-C as well as an increased risk of coronary heart disease (47). Thus, further characterization of how the insulin-FoxO pathway regulates reverse cholesterol transport may (i) improve our understanding of the relationships between insulin resistance, diabetes, and atherogenesis, and (ii) inform clinical decisions about future treatments for diabetes-related cardiovascular disease.

Methods

Mice and Diets

Only adult male mice, 3-5 months old, were studied. L-FoxO1,3,4 mice have been previously described (8, 9). Control mice represent $Foxo1^{flox/flox}$, $Foxo3^{flox/flox}$, and $Foxo4^{flox/Y}$ mice that lack the liver-specific α1-antitrypsin-cre. Mice were fed either standard chow diet (Purina), or WTD containing 42% kcal from fat and 0.2% cholesterol (TD 88137, Harlan Teklad) for 3 weeks. For the adenovirus experiments, mice were injected intravenously with 1×10^8 virus particles/gram of body weight 3 days prior to sacrifice. Murine SR-BI adenovirus was a gift from Dr. Charles M. Rice (77). For the acute FoxO depletion experiments, mice were injected intravenously with 1×10^{11} virus particles/mouse 4 weeks prior to sacrifice. AAV8.Tbg.Cre was a

gift from Dr. Morris Birnbaum. Mice were fasted for 5-hrs on the day of sacrifice, when blood and livers were collected for analysis. Mice are housed in a 12-hr light/dark cycle, with the dark cycle occurring between 7:00 p.m. and 7:00 a.m.

Plasma Lipoprotein Analysis

Total plasma cholesterol was measured using a commercial colorimetric assay (Wako). Plasma lipoproteins were analyzed by running 200 μl of pooled plasma onto a FPLC system consisting of two Superose 6 columns connected in series (Amersham Pharmacia Biotech) as described (78). Fractions for chow-fed mice were collected using fraction collector FC 204 (Gilson), and fractions for WTD-fed mice were collected using fraction collector FRAC-100 (Pharmacia LKB). For western blots of fractionated plasma in both chow-fed and WTD-fed mice, 5 μl from each fraction were pooled in pairs, and were run on a 4%-15% Tris-HCL gradient gel (Bio-Rad), with the exception of adenovirus-injected mice, for which 5μl from each fraction were pooled in groups of 4 or 6, as indicated in the figure. Antibodies to apoA-I and apoE were from Biodesign K23500R and K23100R, respectively.

Gene Expression

Liver RNA was isolated using TRIzol (Invitrogen). cDNA was synthesized using qScript (QuantaBioSciences), and qPCR was performed using SyBr Green (New England Biolabs). Genes were normalized to 36b4. Primer sequences are available in supplemental experimental procedures.

SR-BI expression and HL activity

Liver lysates were prepared in T-PER tissue extraction buffer (ThermoFisher) with added protease inhibitor cocktail (Roche), and immunoblotted for SR-BI (Novus – NB400-104), and beta-Actin (13E5, Cell Signaling – 4970S) as loading control. For western blots of SR-BI in primary hepatocytes, cells were isolated and incubated as described (79). Plasma HL activity was determined as described (34). Briefly, plasma was incubated with 10% Intralipid/[^{3}H]-triolein (Perkin Elmer – NET431L005MC) emulsion as substrate, and human serum as the source of apoCII (80). The contribution of hepatic lipase in the plasma was determined by including NaCl (final concentration 1M) (81). Because heparin was not administered to mice prior to blood collection, the lipase activity was primarily HL (35).

Radiolabeling of HDL

HDL was prepared from wild-type (WT) mice that were fasted 4-hrs before blood harvest. Murine WT-HDL (d = 1.063-1.21 g/ml) was isolated from plasma by sequential ultracentrifugation (82). Murine WT-HDL was double

labeled with ^{125}I-tyramine cellobiose (^{125}I-TC) in the apolipoprotein moiety and with [3H]cholesteryl hexadecyl ether ([3H]CEt) (Perkin Elmer – NET859001MC) in the CE moiety (26, 83). [3H]CEt was introduced in ^{125}I-TC-WT-HDL by exchange from donor liposomal particles, which contained [3H]CEt using human plasma cholesteryl ester transfer protein (84).The final ^{125}I-TC-/[3H]CEt-WT-HDL preparation was extensively dialyzed against PBS (pH 7.4, 4°C) containing EDTA (1 mM).

HDL Metabolism in Mice

For plasma decay analysis of radiolabeled WT-HDL, mice were fasted for 4-hrs before tracer injection (15). Then ^{125}I-TC-/[3H]CEt-WT-HDL (30 µg protein per mouse) was injected via tail vein, and thereafter blood samples (30 µl per time point) were collected periodically (10 and 30 minutes, 2, 7, 22 and 24 hrs) after injection. Animals were fasted throughout the 24-hr study period but had unlimited access to water. Plasma aliquots were directly assayed for ^{125}I radioactivity and [3H] was analyzed after lipid extraction (85). Computer modeling was used to fit (by method of least squares) multiexponential curves, arising from a common two-pool model, simultaneously to both tracers' plasma decay data, and to calculate plasma fractional catabolic rates (plasma-FCR's) for each tracer (86). The modeling was done separately for the data from each mouse, so that individual plasma-FCR's for both tracers were calculated for each animal.

Tissue sites of uptake of HDL-associated tracers were determined 24-hrs after injection of radiolabeled WT-HDL (15). Finally, animals were deeply anesthetized, the abdomen and chest were opened, and a catheter was inserted into the right heart. The inferior vena cava was cut, and the mice were perfused extensively with saline (50 ml per animal). After perfusion, liver, adrenals, kidneys, heart, lungs, spleen, stomach, intestine and carcass from each mouse were harvested and homogenized. Homogenates from each tissue and from carcass were directly assayed for ^{125}I radioactivity, and aliquots were analyzed in parallel for [^{3}H] after lipid extraction (85).

Total radioactivity recovered from all tissues and from the carcass of each mouse was calculated (15). The fraction of total tracer uptake attributed to a specific organ was calculated as the radioactivity recovered in that organ divided by the total radioactivity recovered from all tissues and carcass. Thus the % of recovered extravascular radioactivity in tissues is determined 24-hrs after injection of labeled HDL.

To allow comparison of the specific activities of various tissues in HDL internalization and to directly compare the rates of uptake of the apolipoprotein component and the CE moiety of HDL, the data are expressed as organ fractional catabolic rates (organ-FCR's) (15). These rates are

calculated as follows: (organ-FCR in tissue X) = (Plasma-FCR) x (fraction [%] of total body tracer recovery in tissue X). This organ-FCR represents the fraction of the plasma pool of either HDL tracer cleared by an organ per hour. ^{125}I-TC represents the uptake of HDL holo-particles by tissues (36). Selective HDL CE uptake is calculated as the difference in organ-FCR between [^{3}H]CEt and ^{125}I-TC.

Preparation of murine hepatocytes

Primary hepatocytes were isolated from murine liver by perfusion (37°C, 18 min) with Hanks' balanced salt solution supplemented with collagenase (0.3 mg/ml, type I), HEPES (10 mM), and protease inhibitor mixture "complete" (87). Thereafter, these cells were seeded (37°C, 4.0-hr) in DMEM containing FBS (5%, v/v), penicillin (100 µg/ml) and streptomycin (100 µg/ml). Finally, the culture medium was aspirated, and the cells were washed (PBS, 3x). Hepatocytes were used for ^{125}I-TC-/[^{3}H]CEt-WT-HDL uptake assays. For time course of gene expression in primary hepatocytes, we isolated RNA from hepatocytes at multiple time points during the isolation: (1) Directly after perfusion and before passing the cell suspension through a filter, (2) After the filter, (3) After washing cells, (4) 2-hr after plating, (5) 6-hr after plating, (6) 18-hr after plating, and (7) 24-hr after plating.

Uptake assay for radiolabeled HDL with hepatocytes

To determine cellular uptake of radiolabeled HDL, hepatocytes incubated (37°C, 10, 30 or 120 minutes) in DMEM containing BSA (5 mg/ml), penicillin (100 μg/ml), streptomycin (100 μg/ml) and ^{125}I-TC-/[^{3}H]CEt-WT-HDL (39); the respective incubation time and the concentration of labeled HDL are given in the figure legends. Finally, cells were harvested by trypsin/EDTA (1 x trypsin 0.05 %, EDTA 0.53 mM) treatment, and cellular uptake of HDL tracers was measured. ^{125}I was directly radioassayed, and [^{3}H] was analyzed after lipid extraction (85). Uptake of ^{125}I-TC-/[^{3}H]CEt-WT-HDL by cells is shown in terms of apparent HDL particle uptake, expressed as HDL protein (15, 39). This is done to compare the uptake of both tracers on a common basis. The uptake of HDL holo-particles is represented by ^{125}I-TC, and the difference between [^{3}H]CEt and ^{125}I-TC yields apparent selective HDL CE uptake by cells (36).

Motif Analysis

To determine the number of potential FoxO binding motifs within or near the *Scarb1* and *Lipc* sequences, we obtained the entire mouse gene sequences of *Scarb1* and *Lipc* (including intronic regions), along with 50kb of sequence upstream of each gene's transcription start site. Sequences were obtained from the UCSC Genome Browser (https://genome.ucsc.edu). The sequences were analyzed by the HOMER (Hypergeometric Optimization of Motif

EnRichment) (41) algorithm software, which provided the coordinates of all the potential FoxO binding motifs within this selected region.

Abbreviations

CE, cholesteryl ester; FCR, fractional catabolic rate; FoxO, forkhead box class of transcription factors, family O (including FoxO1, FoxO3, and FoxO4); FPLC, fast protein liquid chromatography; HDL, high density lipoprotein; HDL-C, HDL-cholesterol; HL, hepatic lipase; L-FoxO1,3,4, liver-specific ablation of the three hepatic FoxOs; SR-BI, scavenger receptor class B type I; TC, tyramine cellobiose; WT, Wild-type; WTD, western-type diet

Statistical Analyses

Data are presented as mean ± SEM. Data were analyzed by two-tailed Student's t-tests, or one-way or two-way ANOVA followed by post-hoc test in R, as appropriate. Statistical tests used for each comparison are listed in the figure legends. P value < 0.05 was considered statistically significant.

Study Approval

All animal protocols were approved by the Institutional Animal Care and Use Committees of the University Hospital Hamburg and Columbia College of Physicians and Surgeons, New York, NY.

Author Contributions

R.A.H. conceived of this study, designed and performed experiments, and wrote the paper. S.L. and F.R. designed and performed experiments, and wrote the paper. R.R. analyzed the tracer data. M.H., C.S., G.B., A.W.F., J.H., J.L., and I.H. performed experiments. H.G. and J.H. provided laboratory equipment and contributed to discussions. All authors edited the paper.

References

1. Accili D, and Arden KC. FoxOs at the crossroads of cellular metabolism, differentiation, and transformation. *Cell.* 2004;117(4):421-6.
2. Nakae J, Biggs WH, 3rd, Kitamura T, Cavenee WK, Wright CV, Arden KC, and Accili D. Regulation of insulin action and pancreatic beta-cell function by mutated alleles of the gene encoding forkhead transcription factor Foxo1. *Nat Genet.* 2002;32(2):245-53.
3. Sullivan O, Zhang W, Wasserman DH, Liew CW, Liu J, Paik J, DePinho RA, Stolz DB, Kahn CR, Schwartz MW, et al. FoxO1 integrates direct and indirect effects of insulin on hepatic glucose production and glucose utilization. *Nat Commun.* 2015;6(7079.
4. Lu M, Wan M, Leavens KF, Chu Q, Monks BR, Fernandez S, Ahima RS, Ueki K, Kahn CR, and Birnbaum MJ. Insulin regulates liver metabolism in vivo in the absence of hepatic Akt and Foxo1. *Nat Med.* 2012;18(3):388-95.
5. Dong XC, Copps KD, Guo S, Li Y, Kollipara R, DePinho RA, and White MF. Inactivation of hepatic Foxo1 by insulin signaling is required for adaptive nutrient homeostasis and endocrine growth regulation. *Cell Metab.* 2008;8(1):65-76.
6. Brunet A, Bonni A, Zigmond MJ, Lin MZ, Juo P, Hu LS, Anderson MJ, Arden KC, Blenis J, and Greenberg ME. Akt promotes cell survival by phosphorylating and inhibiting a Forkhead transcription factor. *Cell.* 1999;96(6):857-68.
7. Nakae J, Park BC, and Accili D. Insulin stimulates phosphorylation of the forkhead transcription factor FKHR on serine 253 through a Wortmannin-sensitive pathway. *J Biol Chem.* 1999;274(23):15982-5.
8. Haeusler RA, Kaestner KH, and Accili D. FoxOs function synergistically to promote glucose production. *J Biol Chem.* 2010;285(46):35245-8.
9. Haeusler RA, Hartil K, Vaitheesvaran B, Arrieta-Cruz I, Knight CM, Cook JR, Kammoun HL, Febbraio MA, Gutierrez-Juarez R, Kurland IJ, et al. Integrated control of hepatic lipogenesis versus glucose production requires FoxO transcription factors. *Nat Commun.* 2014;5(5190.
10. Haeusler RA, Pratt-Hyatt M, Welch CL, Klaassen CD, and Accili D. Impaired generation of 12-hydroxylated bile acids links hepatic insulin signaling with dyslipidemia. *Cell Metab.* 2012;15(1):65-74.
11. Zhang W, Patil S, Chauhan B, Guo S, Powell DR, Le J, Klotsas A, Matika R, Xiao X, Franks R, et al. FoxO1 regulates multiple metabolic pathways in the liver: effects on gluconeogenic, glycolytic, and lipogenic gene expression. *J Biol Chem.* 2006;281(15):10105-17.
12. Tao R, Wei D, Gao H, Liu Y, DePinho RA, and Dong XC. Hepatic FoxOs regulate lipid metabolism via modulation of expression of the nicotinamide phosphoribosyltransferase gene. *J Biol Chem.* 2011;286(16):14681-90.
13. Kozarsky KF, Donahee MH, Rigotti A, Iqbal SN, Edelman ER, and Krieger M. Overexpression of the HDL receptor SR-BI alters plasma HDL and bile cholesterol levels. *Nature.* 1997;387(6631):414-7.
14. Rigotti A, Trigatti BL, Penman M, Rayburn H, Herz J, and Krieger M. A targeted mutation in the murine gene encoding the high density lipoprotein (HDL) receptor

scavenger receptor class B type I reveals its key role in HDL metabolism. *Proc Natl Acad Sci U S A.* 1997;94(23):12610-5.

15.   Glass C, Pittman RC, Civen M, and Steinberg D. Uptake of high-density lipoprotein-associated apoprotein A-I and cholesterol esters by 16 tissues of the rat in vivo and by adrenal cells and hepatocytes in vitro. *J Biol Chem.* 1985;260(2):744-50.

16.   Acton S, Rigotti A, Landschulz KT, Xu S, Hobbs HH, and Krieger M. Identification of scavenger receptor SR-BI as a high density lipoprotein receptor. *Science.* 1996;271(5248):518-20.

17.   Jansen H, Verhoeven AJ, and Sijbrands EJ. Hepatic lipase: a pro- or anti-atherogenic protein? *J Lipid Res.* 2002;43(9):1352-62.

18.   Doolittle MH, Wong H, Davis RC, and Schotz MC. Synthesis of hepatic lipase in liver and extrahepatic tissues. *J Lipid Res.* 1987;28(11):1326-34.

19.   Ji ZS, Dichek HL, Miranda RD, and Mahley RW. Heparan sulfate proteoglycans participate in hepatic lipaseand apolipoprotein E-mediated binding and uptake of plasma lipoproteins, including high density lipoproteins. *J Biol Chem.* 1997;272(50):31285-92.

20.   Karackattu SL, Trigatti B, and Krieger M. Hepatic lipase deficiency delays atherosclerosis, myocardial infarction, and cardiac dysfunction and extends lifespan in SR-BI/apolipoprotein E double knockout mice. *Arterioscler Thromb Vasc Biol.* 2006;26(3):548-54.

21.   Amar MJ, Dugi KA, Haudenschild CC, Shamburek RD, Foger B, Chase M, Bensadoun A, Hoyt RF, Jr., Brewer HB, Jr., and Santamarina-Fojo S. Hepatic lipase facilitates the selective uptake of cholesteryl esters from remnant lipoproteins in apoE-deficient mice. *J Lipid Res.* 1998;39(12):2436-42.

22.   Dugi KA, Amar MJ, Haudenschild CC, Shamburek RD, Bensadoun A, Hoyt RF, Jr., Fruchart-Najib J, Madj Z, Brewer HB, Jr., and Santamarina-Fojo S. In vivo evidence for both lipolytic and nonlipolytic function of hepatic lipase in the metabolism of HDL. *Arterioscler Thromb Vasc Biol.* 2000;20(3):793-800.

23.   Dichek HL, Brecht W, Fan J, Ji ZS, McCormick SP, Akeefe H, Conzo L, Sanan DA, Weisgraber KH, Young SG, et al. Overexpression of hepatic lipase in transgenic mice decreases apolipoprotein B-containing and high density lipoproteins. Evidence that hepatic lipase acts as a ligand for lipoprotein uptake. *J Biol Chem.* 1998;273(4):1896-903.

24.   Brundert M, Heeren J, Greten H, and Rinninger F. Hepatic lipase mediates an increase in selective uptake of HDL-associated cholesteryl esters by cells in culture independent from SR-BI. *J Lipid Res.* 2003;44(5):1020-32.

25.   Out R, Hoekstra M, Spijkers JA, Kruijt JK, van Eck M, Bos IS, Twisk J, and Van Berkel TJ. Scavenger receptor class B type I is solely responsible for the selective uptake of cholesteryl esters from HDL by the liver and the adrenals in mice. *J Lipid Res.* 2004;45(11):2088-95.

26.   Brundert M, Ewert A, Heeren J, Behrendt B, Ramakrishnan R, Greten H, Merkel M, and Rinninger F. Scavenger receptor class B type I mediates the selective uptake of high-density lipoprotein-associated cholesteryl ester by the liver in mice. *Arterioscler Thromb Vasc Biol.* 2005;25(1):143-8.

27.   Lambert G, Amar MJ, Martin P, Fruchart-Najib J, Foger B, Shamburek RD, Brewer HB, Jr., and Santamarina-Fojo S. Hepatic lipase deficiency decreases the selective uptake of HDL-cholesteryl esters in vivo. *J Lipid Res.* 2000;41(5):667-72.

28.   Homanics GE, de Silva HV, Osada J, Zhang SH, Wong H, Borensztajn J, and Maeda N. Mild dyslipidemia in mice following targeted inactivation of the hepatic lipase gene. *J Biol Chem.* 1995;270(7):2974-80.

29.   Yamashita S, Sprecher DL, Sakai N, Matsuzawa Y, Tarui S, and Hui DY. Accumulation of apolipoprotein E-rich high density lipoproteins in hyperalphalipoproteinemic human subjects with plasma cholesteryl ester transfer protein deficiency. *J Clin Invest.* 1990;86(3):688-95.

30.   Vaisman BL, Klein HG, Rouis M, Berard AM, Kindt MR, Talley GD, Meyn SM, Hoyt RF, Jr., Marcovina SM, Albers JJ, et al. Overexpression of human lecithin cholesterol acyltransferase leads to hyperalphalipoproteinemia in transgenic mice. *J Biol Chem.* 1995;270(20):12269-75.

31.   Nakashima Y, Plump AS, Raines EW, Breslow JL, and Ross R. ApoE-deficient mice develop lesions of all phases of atherosclerosis throughout the arterial tree. *Arterioscler Thromb.* 1994;14(1):133-40.

32.   Berard AM, Foger B, Remaley A, Shamburek R, Vaisman BL, Talley G, Paigen B, Hoyt RF, Jr., Marcovina S, Brewer HB, Jr., et al. High plasma HDL concentrations associated with enhanced atherosclerosis in transgenic mice overexpressing lecithin-cholesteryl acyltransferase. *Nat Med.* 1997;3(7):744-9.

33.   van Haperen R, van Tol A, van Gent T, Scheek L, Visser P, van der Kamp A, Grosveld F, and de Crom R. Increased risk of atherosclerosis by elevated plasma levels of phospholipid transfer protein. *J Biol Chem.* 2002;277(50):48938-43.

34.   Hocquette JF, Graulet B, and Olivecrona T. Lipoprotein lipase activity and mRNA levels in bovine tissues. *Comp Biochem Physiol B Biochem Mol Biol.* 1998;121(2):201-12.

35.   Peterson J, Bengtsson-Olivecrona G, and Olivecrona T. Mouse preheparin plasma contains high levels of hepatic lipase with low affinity for heparin. *Biochim Biophys Acta.* 1986;878(1):65-70.

36.   Pittman RC, Knecht TP, Rosenbaum MS, and Taylor CA, Jr. A nonendocytotic mechanism for the selective uptake of high density lipoprotein-associated cholesterol esters. *J Biol Chem.* 1987;262(6):2443-50.

37.   Rinninger F, Heine M, Singaraja R, Hayden M, Brundert M, Ramakrishnan R, and Heeren J. High density lipoprotein metabolism in low density lipoprotein receptor-deficient mice. *J Lipid Res.* 2014;55(9):1914-24.

38.   Brundert M, Heeren J, Merkel M, Carambia A, Herkel J, Groitl P, Dobner T, Ramakrishnan R, Moore KJ, and Rinninger F. Scavenger receptor CD36 mediates uptake of high density lipoproteins in mice and by cultured cells. *J Lipid Res.* 2011;52(4):745-58.

39.   Rinninger F, Brundert M, Jackle S, Galle PR, Busch C, Izbicki JR, Rogiers X, Henne-Bruns D, Kremer B, Broelsch CE, et al. Selective uptake of high-density lipoprotein-associated cholesteryl esters by human hepatocytes in primary culture. *Hepatology.* 1994;19(5):1100-14.

40.   Tsukamoto K, Buck L, Inman W, Griffith L, Kocher O, and Krieger M. Challenges in using cultured primary rodent hepatocytes or cell lines to study hepatic HDL

receptor SR-BI regulation by its cytoplasmic adaptor PDZK1. *PLoS One.*
2013;8(7):e69725.

41.   Heinz S, Benner C, Spann N, Bertolino E, Lin YC, Laslo P, Cheng JX, Murre C, Singh H,
and Glass CK. Simple combinations of lineage-determining transcription factors
prime cis-regulatory elements required for macrophage and B cell identities. *Mol
Cell.* 2010;38(4):576-89.

42.   Ikemoto M, Arai H, Feng D, Tanaka K, Aoki J, Dohmae N, Takio K, Adachi H,
Tsujimoto M, and Inoue K. Identification of a PDZ-domain-containing protein that
interacts with the scavenger receptor class B type I. *Proc Natl Acad Sci U S A.*
2000;97(12):6538-43.

43.   Kocher O, Yesilaltay A, Cirovic C, Pal R, Rigotti A, and Krieger M. Targeted disruption
of the PDZK1 gene in mice causes tissue-specific depletion of the high density
lipoprotein receptor scavenger receptor class B type I and altered lipoprotein
metabolism. *J Biol Chem.* 2003;278(52):52820-5.

44.   Lambert G, Chase MB, Dugi K, Bensadoun A, Brewer HB, Jr., and Santamarina-Fojo S.
Hepatic lipase promotes the selective uptake of high density lipoprotein-cholesteryl
esters via the scavenger receptor B1. *J Lipid Res.* 1999;40(7):1294-303.

45.   Teslovich TM, Musunuru K, Smith AV, Edmondson AC, Stylianou IM, Koseki M,
Pirruccello JP, Ripatti S, Chasman DI, Willer CJ, et al. Biological, clinical and
population relevance of 95 loci for blood lipids. *Nature.* 2010;466(7307):707-13.

46.   Kathiresan S, Melander O, Guiducci C, Surti A, Burtt NP, Rieder MJ, Cooper GM, Roos
C, Voight BF, Havulinna AS, et al. Six new loci associated with blood low-density
lipoprotein cholesterol, high-density lipoprotein cholesterol or triglycerides in
humans. *Nat Genet.* 2008;40(2):189-97.

47.   Zanoni P, Khetarpal SA, Larach DB, Hancock-Cerutti WF, Millar JS, Cuchel M,
DerOhannessian S, Kontush A, Surendran P, Saleheen D, et al. Rare variant in
scavenger receptor BI raises HDL cholesterol and increases risk of coronary heart
disease. *Science.* 2016;351(6278):1166-71.

48.   Demant T, Carlson LA, Holmquist L, Karpe F, Nilsson-Ehle P, Packard CJ, and
Shepherd J. Lipoprotein metabolism in hepatic lipase deficiency: studies on the
turnover of apolipoprotein B and on the effect of hepatic lipase on high density
lipoprotein. *J Lipid Res.* 1988;29(12):1603-11.

49.   Carlson LA, Holmquist L, and Nilsson-Ehle P. Deficiency of hepatic lipase activity in
post-heparin plasma in familial hyper-alpha-triglyceridemia. *Acta Med Scand.*
1986;219(5):435-47.

50.   Breckenridge WC, Little JA, Alaupovic P, Wang CS, Kuksis A, Kakis G, Lindgren F, and
Gardiner G. Lipoprotein abnormalities associated with a familial deficiency of
hepatic lipase. *Atherosclerosis.* 1982;45(2):161-79.

51.   Graf GA, Yu L, Li WP, Gerard R, Tuma PL, Cohen JC, and Hobbs HH. ABCG5 and
ABCG8 are obligate heterodimers for protein trafficking and biliary cholesterol
excretion. *J Biol Chem.* 2003;278(48):48275-82.

52.   Yu L, Gupta S, Xu F, Liverman AD, Moschetta A, Mangelsdorf DJ, Repa JJ, Hobbs HH,
and Cohen JC. Expression of ABCG5 and ABCG8 is required for regulation of biliary
cholesterol secretion. *J Biol Chem.* 2005;280(10):8742-7.

53.   Schwarz M, Lund EG, Setchell KD, Kayden HJ, Zerwekh JE, Bjorkhem I, Herz J, and
Russell DW. Disruption of cholesterol 7alpha-hydroxylase gene in mice. II. Bile acid

deficiency is overcome by induction of oxysterol 7alpha-hydroxylase. *The Journal of biological chemistry.* 1996;271(30):18024-31.

54.   Russell DW. The enzymes, regulation, and genetics of bile acid synthesis. *Annual review of biochemistry.* 2003;72(137-74.

55.   Biddinger SB, Haas JT, Yu BB, Bezy O, Jing E, Zhang W, Unterman TG, Carey MC, and Kahn CR. Hepatic insulin resistance directly promotes formation of cholesterol gallstones. *Nat Med.* 2008;14(7):778-82.

56.   Shin DJ, and Osborne TF. FGF15/FGFR4 integrates growth factor signaling with hepatic bile acid metabolism and insulin action. *J Biol Chem.* 2009;284(17):11110-20.

57.   Li T, Kong X, Owsley E, Ellis E, Strom S, and Chiang JY. Insulin regulation of cholesterol 7alpha-hydroxylase expression in human hepatocytes: roles of forkhead box O1 and sterol regulatory element-binding protein 1c. *J Biol Chem.* 2006;281(39):28745-54.

58.   Li T, Ma H, Park YJ, Lee YK, Strom S, Moore DD, and Chiang JY. Forkhead box transcription factor O1 inhibits cholesterol 7alpha-hydroxylase in human hepatocytes and in high fat diet-fed mice. *Biochim Biophys Acta.* 2009;1791(10):991-6.

59.   Nakae J, Kitamura T, Silver DL, and Accili D. The forkhead transcription factor Foxo1 (Fkhr) confers insulin sensitivity onto glucose-6-phosphatase expression. *J Clin Invest.* 2001;108(9):1359-67.

60.   Biddinger SB, Hernandez-Ono A, Rask-Madsen C, Haas JT, Aleman JO, Suzuki R, Scapa EF, Agarwal C, Carey MC, Stephanopoulos G, et al. Hepatic insulin resistance is sufficient to produce dyslipidemia and susceptibility to atherosclerosis. *Cell Metab.* 2008;7(2):125-34.

61.   Matsumoto M, Pocai A, Rossetti L, Depinho RA, and Accili D. Impaired regulation of hepatic glucose production in mice lacking the forkhead transcription factor Foxo1 in liver. *Cell Metab.* 2007;6(3):208-16.

62.   Ai D, Chen C, Han S, Ganda A, Murphy AJ, Haeusler R, Thorp E, Accili D, Horton JD, and Tall AR. Regulation of hepatic LDL receptors by mTORC1 and PCSK9 in mice. *J Clin Invest.* 2012;122(4):1262-70.

63.   Crestani M, Stroup D, and Chiang JY. Hormonal regulation of the cholesterol 7 alpha-hydroxylase gene (CYP7). *J Lipid Res.* 1995;36(11):2419-32.

64.   Gibbons GF. Regulation of fatty acid and cholesterol synthesis: co-operation or competition? *Prog Lipid Res.* 2003;42(6):479-97.

65.   Lin HV, and Accili D. Hormonal regulation of hepatic glucose production in health and disease. *Cell Metab.* 2011;14(1):9-19.

66.   Krauss RM. Lipids and lipoproteins in patients with type 2 diabetes. *Diabetes Care.* 2004;27(6):1496-504.

67.   Baynes C, Henderson AD, Anyaoku V, Richmond W, Hughes CL, Johnston DG, and Elkeles RS. The role of insulin insensitivity and hepatic lipase in the dyslipidaemia of type 2 diabetes. *Diabet Med.* 1991;8(6):560-6.

68.   Berk P, II, Hoogerbrugge N, Stolk RP, Bootsma AH, Jansen H, and Group DS. Atorvastatin dose-dependently decreases hepatic lipase activity in type 2 diabetes: effect of sex and the LIPC promoter variant. *Diabetes Care.* 2003;26(2):427-32.

69. Arai T, Rinninger F, Varban L, Fairchild-Huntress V, Liang CP, Chen W, Seo T, Deckelbaum R, Huszar D, and Tall AR. Decreased selective uptake of high density lipoprotein cholesteryl esters in apolipoprotein E knock-out mice. *Proc Natl Acad Sci U S A.* 1999;96(21):12050-5.

70. Thuren T, Sisson P, and Waite M. Activation of hepatic lipase catalyzed phosphatidylcholine hydrolysis by apolipoprotein E. *Biochim Biophys Acta.* 1991;1083(2):217-20.

71. Thuren T, Weisgraber KH, Sisson P, and Waite M. Role of apolipoprotein E in hepatic lipase catalyzed hydrolysis of phospholipid in high-density lipoproteins. *Biochemistry.* 1992;31(8):2332-8.

72. Van Eck M, Twisk J, Hoekstra M, Van Rij BT, Van der Lans CA, Bos IS, Kruijt JK, Kuipers F, and Van Berkel TJ. Differential effects of scavenger receptor BI deficiency on lipid metabolism in cells of the arterial wall and in the liver. *J Biol Chem.* 2003;278(26):23699-705.

73. Lewis GF, and Rader DJ. New insights into the regulation of HDL metabolism and reverse cholesterol transport. *Circ Res.* 2005;96(12):1221-32.

74. Tall AR. An overview of reverse cholesterol transport. *Eur Heart J.* 1998;19 Suppl A(A31-5.

75. Rader DJ, Alexander ET, Weibel GL, Billheimer J, and Rothblat GH. The role of reverse cholesterol transport in animals and humans and relationship to atherosclerosis. *J Lipid Res.* 2009;50 Suppl(S189-94.

76. Rader DJ, and Tall AR. The not-so-simple HDL story: Is it time to revise the HDL cholesterol hypothesis? *Nat Med.* 2012;18(9):1344-6.

77. Dorner M, Horwitz JA, Robbins JB, Barry WT, Feng Q, Mu K, Jones CT, Schoggins JW, Catanese MT, Burton DR, et al. A genetically humanized mouse model for hepatitis C virus infection. *Nature.* 2011;474(7350):208-11.

78. Jiao S, Cole TG, Kitchens RT, Pfleger B, and Schonfeld G. Genetic heterogeneity of lipoproteins in inbred strains of mice: analysis by gel-permeation chromatography. *Metabolism.* 1990;39(2):155-60.

79. Cook JR, Matsumoto M, Banks AS, Kitamura T, Tsuchiya K, and Accili D. A mutant allele encoding DNA binding-deficient FoxO1 differentially regulates hepatic glucose and lipid metabolism. *Diabetes.* 2015;64(6):1951-65.

80. Nilsson-Ehle P, and Schotz MC. A stable, radioactive substrate emulsion for assay of lipoprotein lipase. *J Lipid Res.* 1976;17(5):536-41.

81. Henderson AD, Richmond W, and Elkeles RS. Hepatic and lipoprotein lipases selectively assayed in postheparin plasma. *Clin Chem.* 1993;39(2):218-23.

82. Havel RJ, Eder HA, and Bragdon JH. The distribution and chemical composition of ultracentrifugally separated lipoproteins in human serum. *J Clin Invest.* 1955;34(9):1345-53.

83. Pittman RC, and Taylor CA, Jr. Methods for assessment of tissue sites of lipoprotein degradation. *Methods Enzymol.* 1986;129(612-28.

84. Morton RE, and Zilversmit DB. Inter-relationship of lipids transferred by the lipid-transfer protein isolated from human lipoprotein-deficient plasma. *J Biol Chem.* 1983;258(19):11751-7.

85. Dole VP. A relation between non-esterified fatty acids in plasma and the metabolism of glucose. *J Clin Invest.* 1956;35(2):150-4.

86. Le NA, Ramakrishnan R, Dell RB, Ginsberg HN, and Brown WV. Kinetic analysis using specific radioactivity data. *Methods Enzymol.* 1986;129(384-95.

87. Silver DL, Wang N, and Tall AR. Defective HDL particle uptake in ob/ob hepatocytes causes decreased recycling, degradation, and selective lipid uptake. *J Clin Invest.* 2000;105(2):151-9.

Table 1: HDL Metabolism of L-FoxO1,3,4 Mice							
		Control Mice Chow			L-FoxO1,3,4 Mice Chow		
		^{125}I	$[^3H]$	$[^3H]$-^{125}I	^{125}I	$[^3H]$	$[^3H]$-^{125}I
Plasma-FCR's x h^{-1}		0.052±0.008	0.133±0.011	0.0811±0.006	0.049±0.003	0.0844±0.007*	0.0354±0.004*
Organ-FCR's x h^{-1} x 10^3	Spleen	0.31±0.057	4.13±0.64	3.82±0.59	0.32 ± 0.022	2.30 ± 0.15*	1.38 ± 0.14*
	Stomach	1.90±0.23	1.27±0.24		1.01±0.14*	0.348±0.060*	
	Intestine	7.3±1.2	4.0±0.52		7.5±0.7	2.5±0.27*	
	Heart	0.35±0.064	0.25±0.035		0.32±0.013	0.20±0.016	
	Lungs	0.55±0.11	0.64±0.088		0.57±0.059	0.49±0.039	
	Carcass	27.4±4.3	25.4±2.5		24.8±1.4	18.6±1.3*	

Table 1 Plasma-FCRs and Tracer Uptake Rates by Tissues for ^{125}I-TC-/[^{3}H]CEt-WT-HDL in Chow-Fed L-FoxO1,3,4 mice

^{125}I-TC-/[^{3}H]CEt-WT-HDL was injected intravenously in chow-fed L-FoxO1,3,4 mice and littermate controls. During the subsequent 24-hr interval, blood was harvested periodically to determine the plasma decay of both tracers. ^{125}I-TC (^{125}I) and [^{3}H]CEt ([^{3}H]) were analyzed, and plasma-FCRs for ^{125}I-TC and [^{3}H]CEt were calculated. The difference in plasma-FCRs between [^{3}H]CEt and ^{125}I-TC was calculated. 24-hrs after tracer injection, the animals were euthanized, and tissues were analyzed for both tracers. Spleen, stomach, intestine, heart, lungs and carcass organ-FCRs for ^{125}I-TC (^{125}I), [^{3}H]CEt ([^{3}H]), and the difference in organ-FCRs between [^{3}H]CEt and ^{125}I-TC ([^{3}H]CEt - ^{125}I-TC) were calculated. All calculations were done as described in Materials and Methods. For control mice, values are means ± SEM of n = 7 mice and for L-FoxO1,3,4 mice n = 5. An independent experiment yielded qualitatively identical results. *p < 0.05 by Student's t-tests.
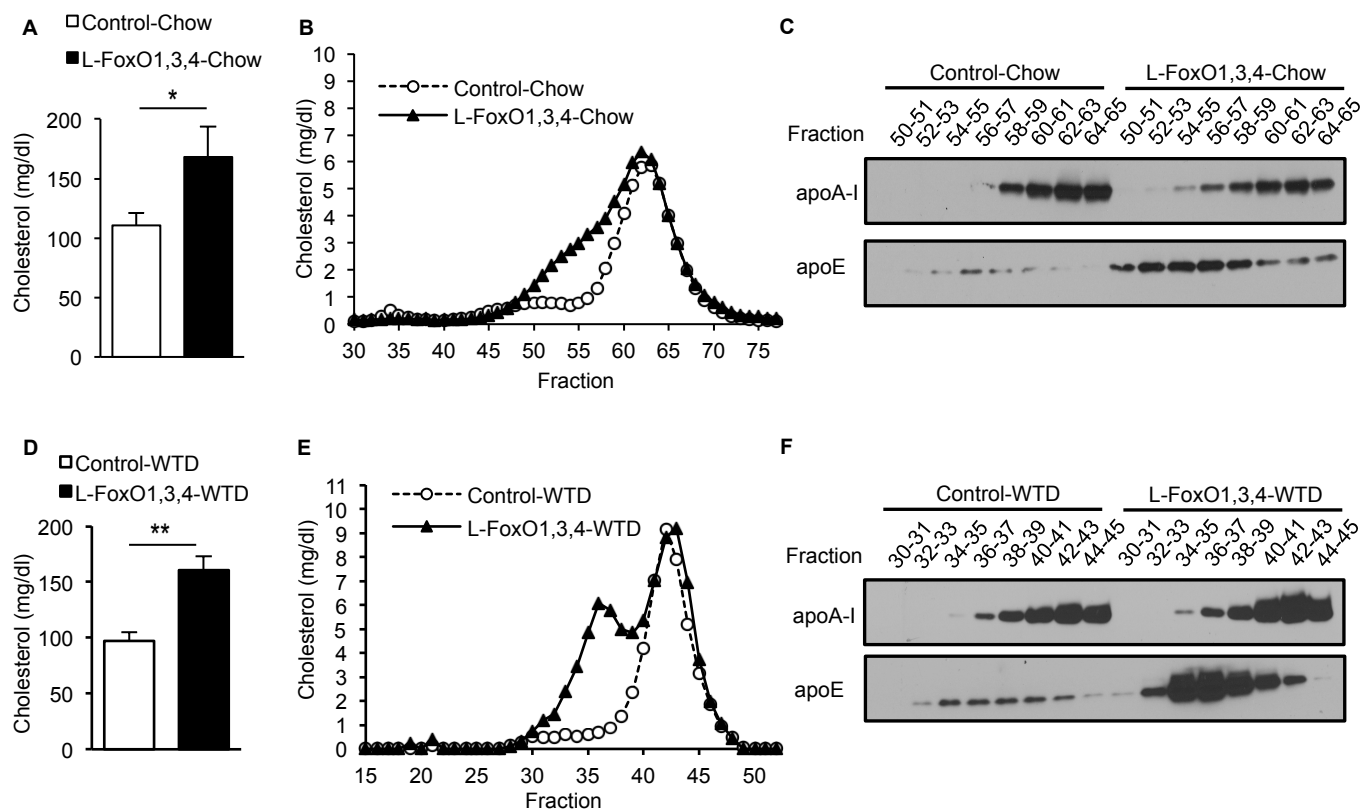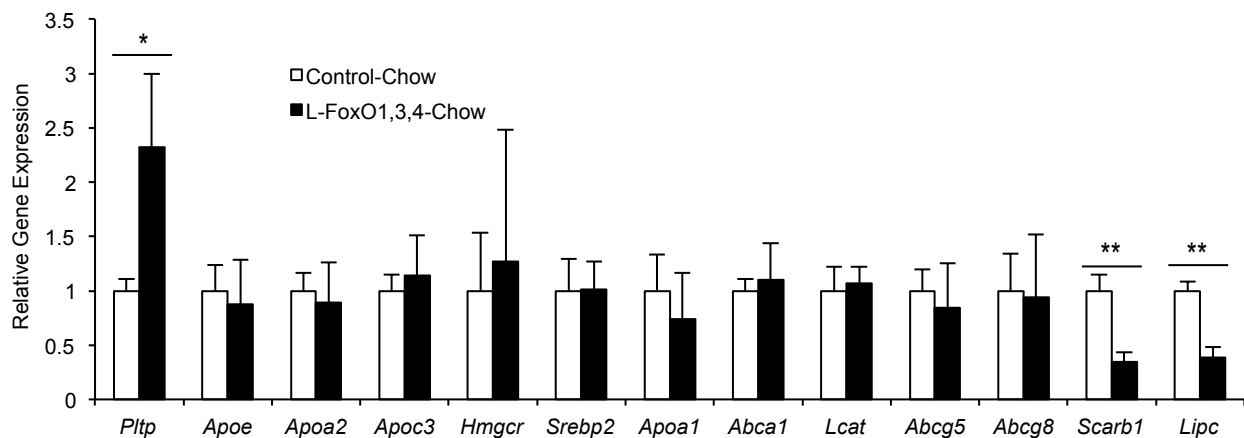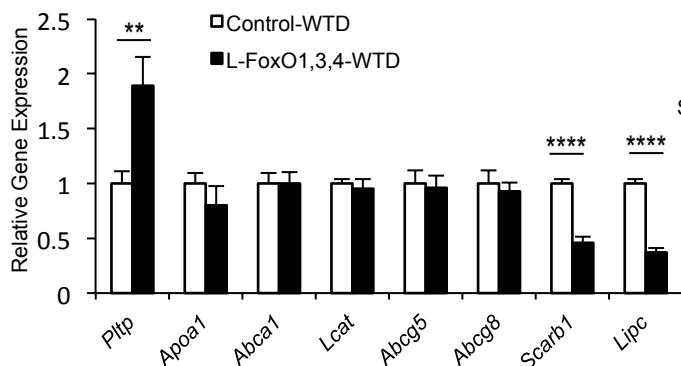
Figure 1. Plasma Cholesterol Profiles of Chow-fed and WTD-fed L-FoxO1,3,4 Mice
(A) Total plasma cholesterol in chow-fed L-FoxO1,3,4 mice and littermate controls after a 5-hr fast
(n=5). Data are presented as mean ± SEM. (B) Cholesterol levels in plasma fractionated by FPLC in
same mice as 1A. (C) Western blot of plasma apoA-I and apoE from pooled pairs of fractionated
plasma obtained from FPLC in 1B. (D) Total plasma cholesterol in WTD-fed L-FoxO1,3,4 mice and
littermate controls after a 5-hr fast (n=5). Data are presented as mean ± SEM. (E) Cholesterol levels in
plasma fractionated by FPLC in same mice as 1D. (F) Western blot of plasma apoA-I and apoE from
pooled pairs of fractionated plasma obtained from FPLC in 1E. Independent FPLC-cholesterol profiles
for both chow-fed and WTD-fed mice yielded qualitatively identical results. *p < 0.05, **p < 0.01 by
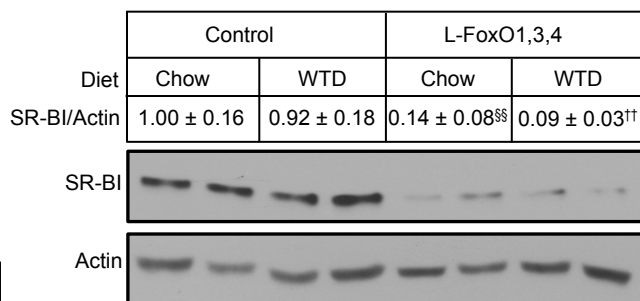Student's t-test.

A

B

C

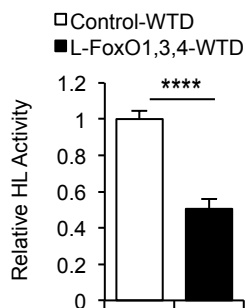| Diet	Control		L-FoxO1,3,4	
	Chow	WTD	Chow	WTD
SR-BI/Actin	1.00 ± 0.16	0.92 ± 0.18	0.14 ± 0.08§§	0.09 ± 0.03††

SR-BI

Actin

D

Figure 2. Defects in HDL Metabolism Genes Due to Ablation of Hepatic FoxOs
(A-B) Relative hepatic gene expression by qPCR in (A) chow-fed L-FoxO1,3,4 mice
and littermate controls (n=4-5), and in (B) WTD-fed L-FoxO1,3,4 mice and littermate
controls (n=6-7). (C) Representative western blot of hepatic SR-BI expression in both
chow-fed and WTD-fed L-FoxO1,3,4 mice and littermate controls. SR-BI/Actin
denotes relative SR-BI expression levels by densitometric scanning (n=4 per group
total). (D) Relative plasma hepatic lipase activity in WTD-fed L-FoxO1,3,4 mice and
littermate controls (n=5-7). *$p < 0.05$, **$p < 0.01$, ***$p < 0.001$, ****$p < 0.0001$; §§$p <
0.01$ between chow-fed L-FoxO1,3,4 mice and littermate controls; ††$p < 0.01$
between WTD-fed L-FoxO1,3,4 mice and littermate controls by Student's t-tests.
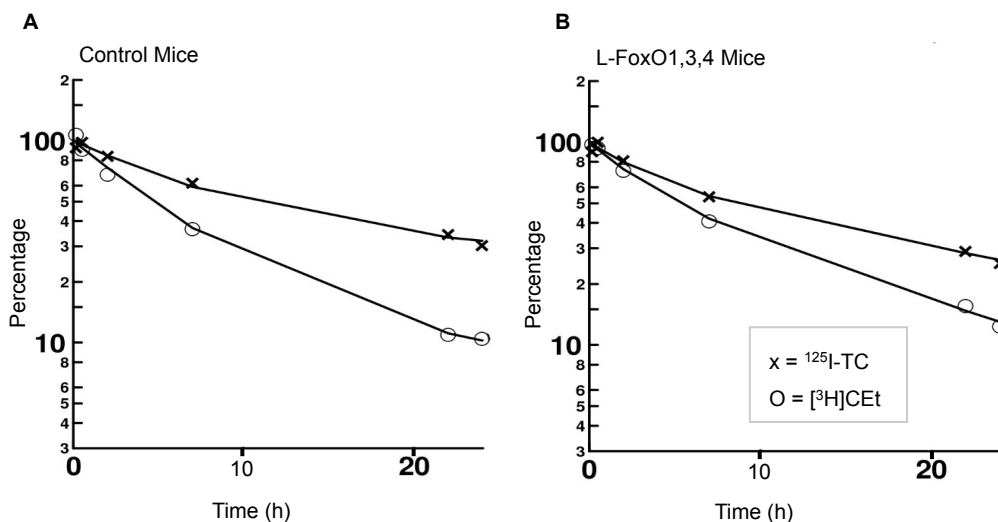Data are presented as mean ± SEM.

Figure 3. Plasma Decay Kinetics of ^{125}I-TC-/[3H]CEt-WT-HDL in Chow-Fed L-FoxO1,3,4 Mice
(A-B) ^{125}I-TC-/[3H]CEt-WT-HDL was injected intravenously in chow-fed L-FoxO1,3,4 mice and littermate controls. Thereafter, during a 24-hr interval, periodic blood samples were harvested and plasma was analyzed for ^{125}I-TC (crosses) and [3H]CEt (circles). The y-axis represents the fraction of the tracer in plasma (%). Shown is a trace from a representative mouse from each genotype, with (A) control on the left and (B) L-FoxO1,3,4 on the right. The experiment was carried out in 7 control and 5 L-FoxO1,3,4 mice.
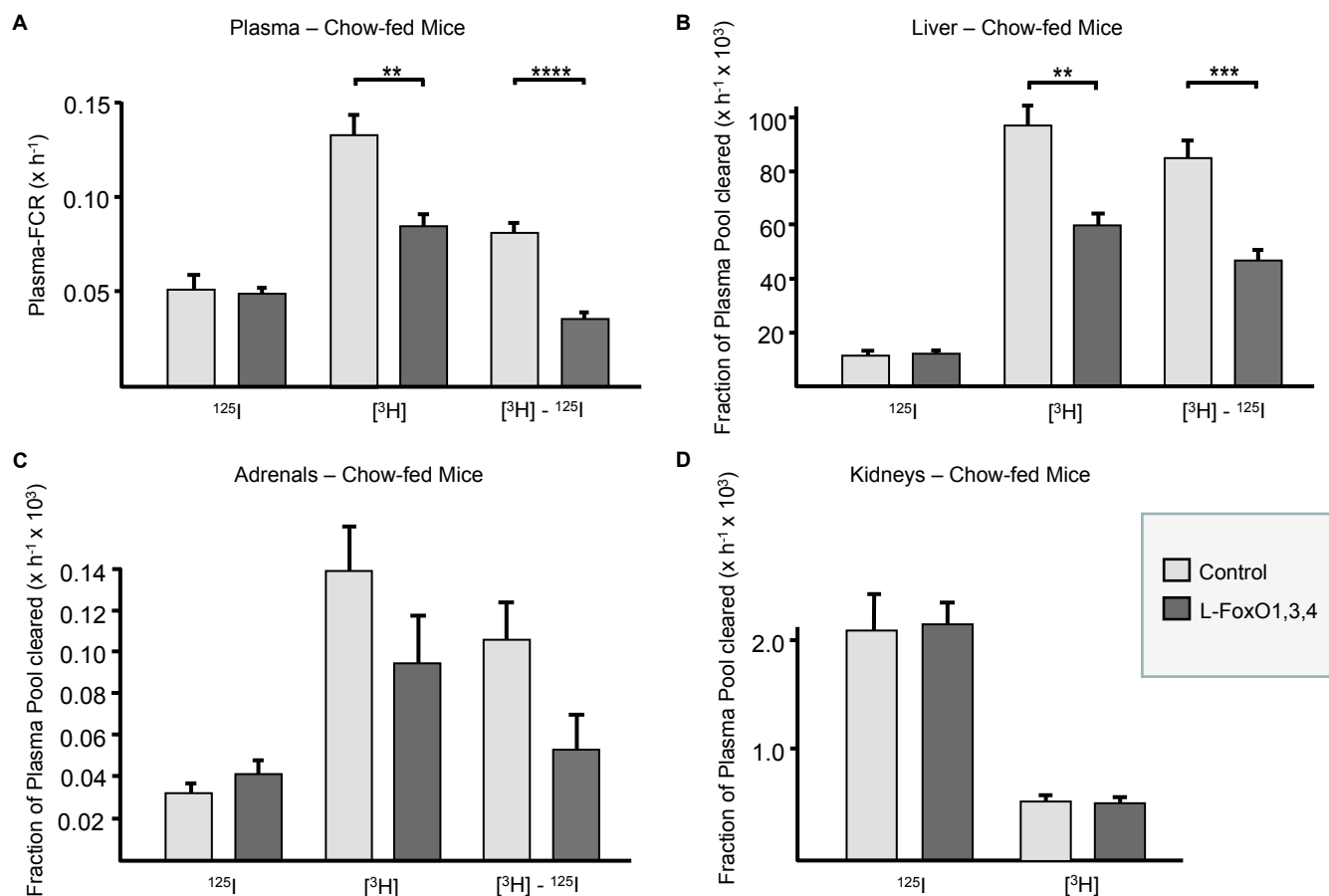
Figure 4. Plasma-FCRs and Tissue Tracer Uptake Rates for ^{125}I-TC-/[^{3}H]CEt-WT-HDL in Chow-Fed L-FoxO1,3,4 Mice

^{125}I-TC-/[^{3}H]CEt-WT-HDL was injected intravenously in chow-fed L-FoxO1,3,4 mice and littermate controls. (A) During the subsequent 24-hr interval, blood was harvested periodically to determine the plasma decay of both tracers. ^{125}I-TC (^{125}I) and [^{3}H]CEt ([^{3}H]) were analyzed, and plasma-FCRs for ^{125}I-TC and [^{3}H]CEt were calculated. The difference in plasma-FCRs between [^{3}H]CEt and ^{125}I-TC was calculated. 24-hrs after tracer injection, the animals were euthanized, and tissues were analyzed for both tracers. (B) Liver, (C) adrenal and (D) kidney organ-FCRs for ^{125}I-TC (^{125}I), [^{3}H]CEt ([^{3}H]), and the difference in organ-FCRs between [^{3}H]CEt and ^{125}I-TC ([^{3}H]CEt - ^{125}I-TC) were calculated. All calculations were done as described in Materials and Methods. n = 7 control and n = 5 L-FoxO1,3,4 mice. An independent experiment yielded qualitatively identical results. **p < 0.01, ***p < 0.001, ****p < 0.0001 by Student's t-tests. In adrenal glands, there were no significant differences between genotypes. Data are presented as mean ± SEM.
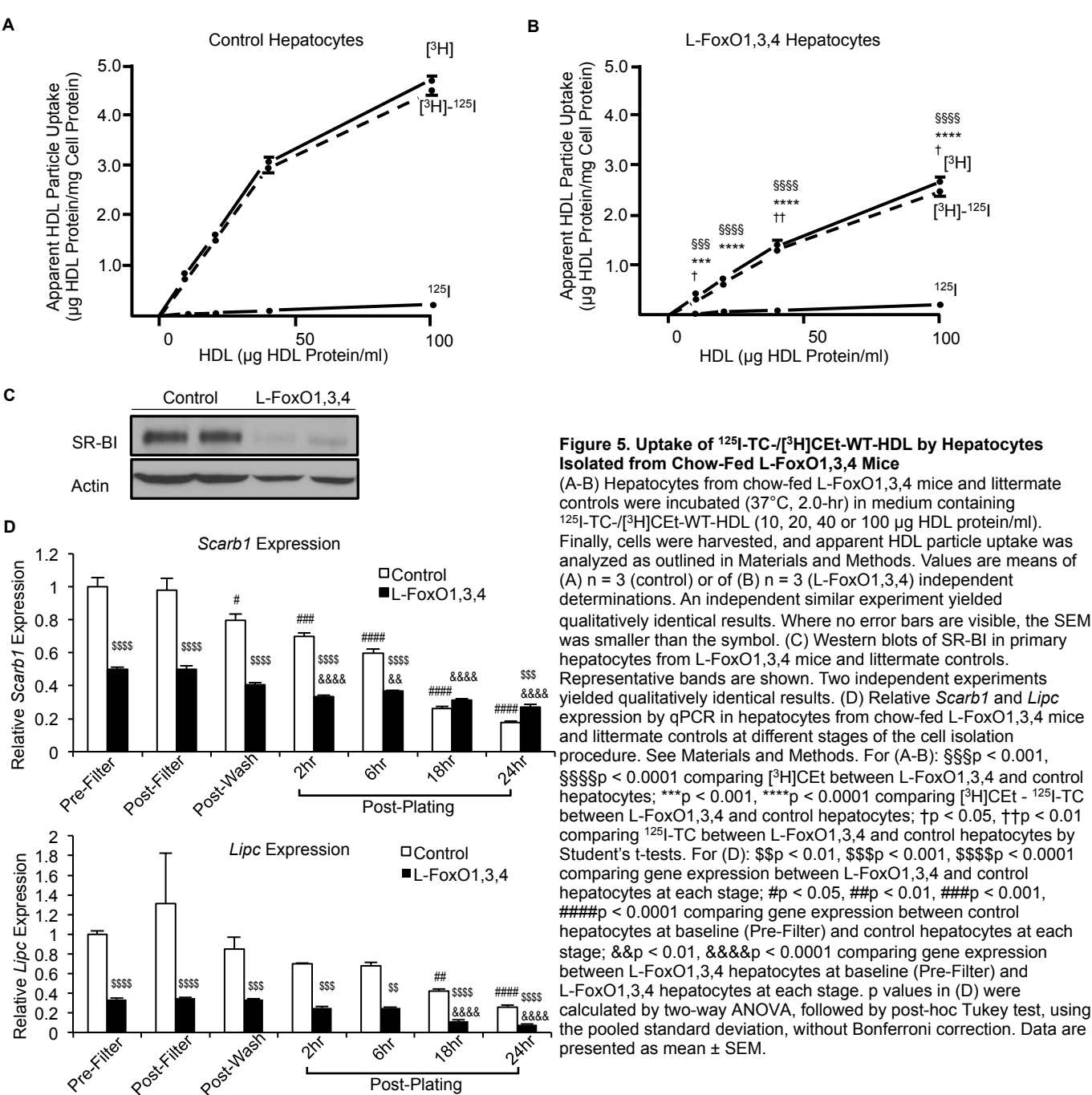
A Control Hepatocytes

B L-FoxO1,3,4 Hepatocytes

C

D

Scarb1 Expression

Lipc Expression

Figure 5. Uptake of ^{125}I-TC-/[3H]CEt-WT-HDL by Hepatocytes Isolated from Chow-Fed L-FoxO1,3,4 Mice

(A-B) Hepatocytes from chow-fed L-FoxO1,3,4 mice and littermate controls were incubated (37°C, 2.0-hr) in medium containing ^{125}I-TC-/[3H]CEt-WT-HDL (10, 20, 40 or 100 μg HDL protein/ml). Finally, cells were harvested, and apparent HDL particle uptake was analyzed as outlined in Materials and Methods. Values are means of (A) n = 3 (control) or of (B) n = 3 (L-FoxO1,3,4) independent determinations. An independent similar experiment yielded qualitatively identical results. Where no error bars are visible, the SEM was smaller than the symbol. (C) Western blots of SR-BI in primary hepatocytes from L-FoxO1,3,4 mice and littermate controls. Representative bands are shown. Two independent experiments yielded qualitatively identical results. (D) Relative *Scarb1* and *Lipc* expression by qPCR in hepatocytes from chow-fed L-FoxO1,3,4 mice and littermate controls at different stages of the cell isolation procedure. See Materials and Methods. For (A-B): §§§$p < 0.001$, §§§§$p < 0.0001$ comparing [3H]CEt between L-FoxO1,3,4 and control hepatocytes; ***$p < 0.001$, ****$p < 0.0001$ comparing [3H]CEt - ^{125}I-TC between L-FoxO1,3,4 and control hepatocytes; †$p < 0.05$, ††$p < 0.01$ comparing ^{125}I-TC between L-FoxO1,3,4 and control hepatocytes by Student's t-tests. For (D): $$$p < 0.01$, $$$$p < 0.001$, $$$$$p < 0.0001$ comparing gene expression between L-FoxO1,3,4 and control hepatocytes at each stage; #$p < 0.05$, ##$p < 0.01$, ###$p < 0.001$, ####$p < 0.0001$ comparing gene expression between control hepatocytes at baseline (Pre-Filter) and control hepatocytes at each stage; &&$p < 0.01$, &&&&$p < 0.0001$ comparing gene expression between L-FoxO1,3,4 hepatocytes at baseline (Pre-Filter) and L-FoxO1,3,4 hepatocytes at each stage. p values in (D) were calculated by two-way ANOVA, followed by post-hoc Tukey test, using the pooled standard deviation, without Bonferroni correction. Data are presented as mean ± SEM.
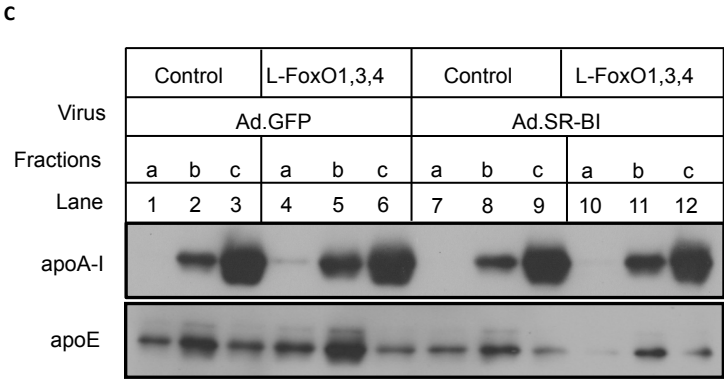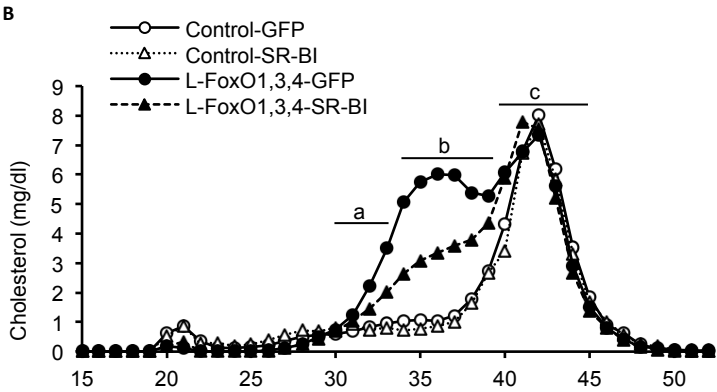
A

	Control-WTD		L-FoxO1,3,4-WTD	
Virus	Ad.GFP	Ad.SR-BI	Ad.GFP	Ad.SR-BI
SR-BI/ Actin	1.00 ± 0.09	1.16 ± 0.09	0.11 ± 0.05	0.55 ± 0.05

SR-BI

Actin

B

C

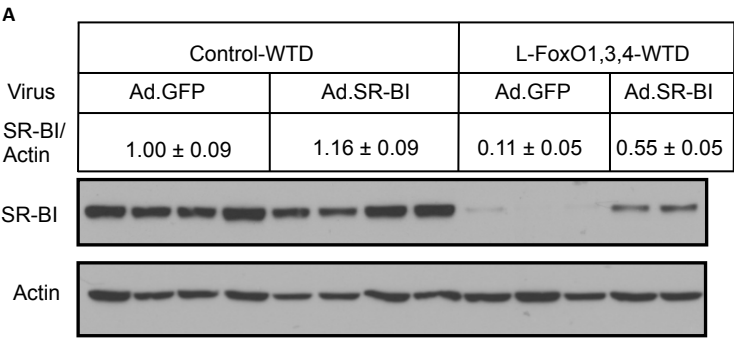|	Control	L-FoxO1,3,4	Control	L-FoxO1,3,4
Virus	Ad.GFP		Ad.SR-BI	
Fractions	a b c	a b c	a b c	a b c
Lane	1 2 3	4 5 6	7 8 9	10 11 12

apoA-I

apoE

Figure 6. SR-BI Adenovirus in WTD-fed L-FoxO1,3,4 Mice
(A) Western blot of hepatic SR-BI expression in WTD-fed L-FoxO1,3,4 mice and littermate controls transduced with Ad.SR-BI or control virus (Ad.GFP). SR-BI/Actin denotes relative SR-BI expression levels by densitometric scanning (n=2-4). (B) Cholesterol levels in plasma fractionated by FPLC in same mice as 6A. (C) Western blot of plasma apoA-I and apoE in fractionated plasma obtained from FPLC in 6B. Lanes "a, b, c," correspond to pooled fractions from lanes "30-33, 34-39, 40-45," respectively.
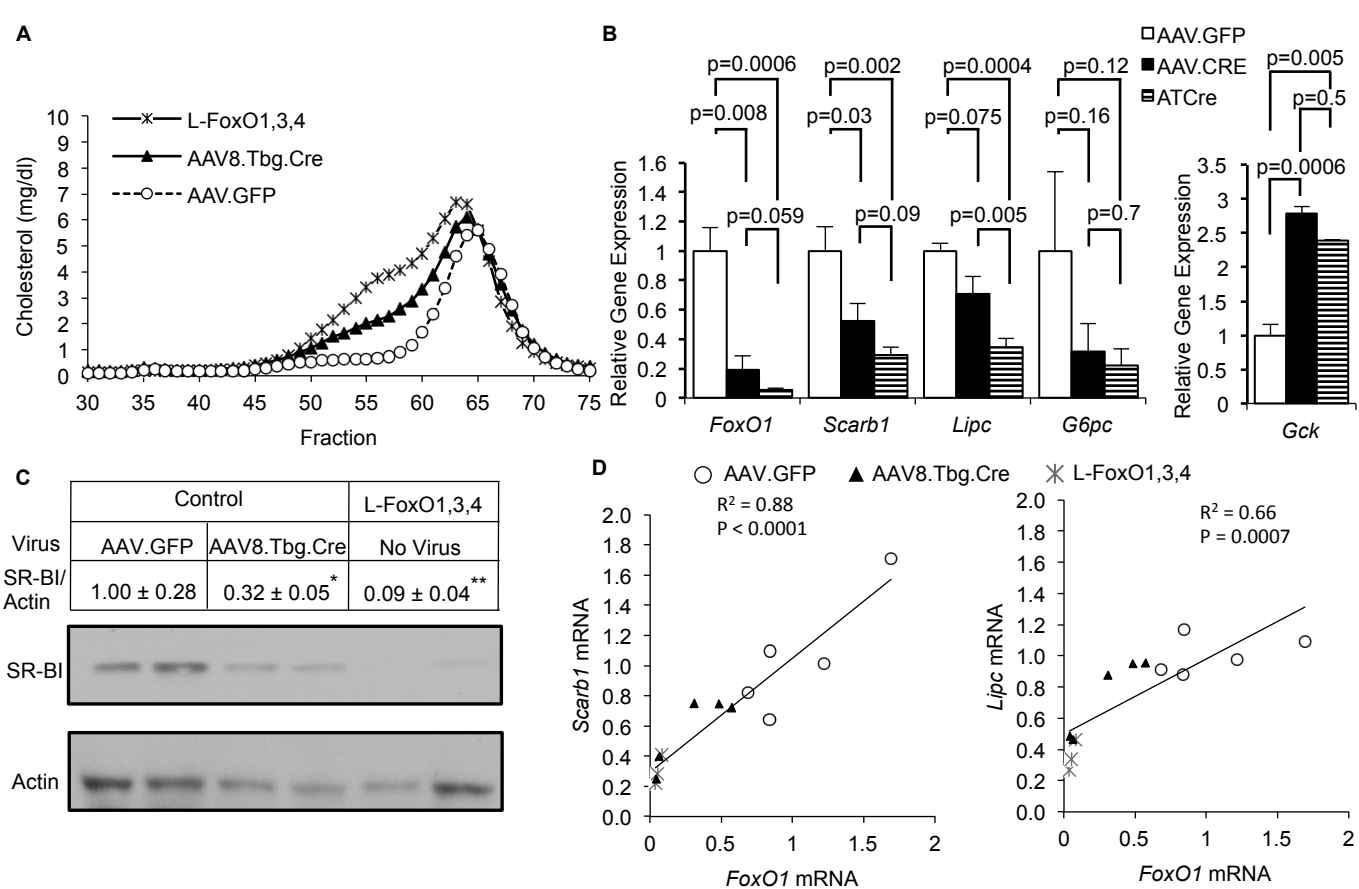
Figure 7. Acute Knockdown via Cre Adeno-Associated virus in Chow-fed Hepatic FoxO Floxed Mice
(A-D) Chow-fed, adult *Foxo1^flox/flox^*, *Foxo3^flox/flox^*, and *Foxo4^flox/Y^* control mice transduced with adeno-associated virus (serotype 8) expressing Cre recombinase driven by the hepatocyte-specific Tbg promoter (AAV8.Tbg.Cre) or control virus (AAV.GFP) (n=5). For comparison, we also included a group of traditional L-FoxO1,3,4 knockout mice that were not transduced with virus, but rather had FoxO deficiency since birth (n=4). Four weeks after virus transduction, mice were fasted for 5-hrs and then plasma and livers were collected. (A) Cholesterol levels in plasma fractionated by FPLC 4 weeks after virus transduction. (B) Relative hepatic gene expression by qPCR. (C) Representative western blot of hepatic SR-BI expression. SR-BI/Actin denotes relative SR-BI expression levels by densitometric scanning. *p < 0.05, **p < 0.01 compared to AAV.GFP mice. Between AAV8.Tbg.Cre mice and L-FoxO1,3,4 mice, there was no significant difference. (D) Correlation between *Scarb1* or *Lipc* mRNA with *FoxO1* mRNA. p values in (B) and (C) were calculated by one-way ANOVA, followed by post-hoc t-test, using the pooled standard deviation, without Bonferroni correction. Data are presented as mean ± SEM.
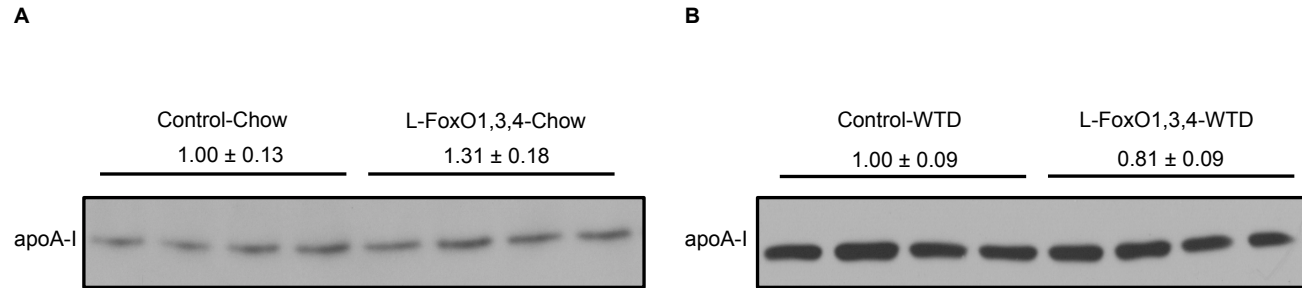
Supplemental Figure S1

A

Control-Chow	L-FoxO1,3,4-Chow
1.00 ± 0.13	1.31 ± 0.18

apoA-I

B

Control-WTD	L-FoxO1,3,4-WTD
1.00 ± 0.09	0.81 ± 0.09

apoA-I

Figure S1. Western Blot of Total Plasma apoA-I. Related to Figure 1
(A-B) Plasma was collected from (A) chow-fed and (B) WTD-fed L-FoxO1,3,4 mice and littermate controls. Plasma was diluted by 1:200 with PBS, from which 20µl from each sample were run on a 4%-15% Tris-HCL gradient gel and blotted for apoA-I. Numbers denote relative apoA-I expression levels by densitometric scanning (n=4-7). Values are presented as mean ± SEM. Shown is a typical experiment. Independent experiments yielded qualitatively identical results.

Supplemental Figure S2

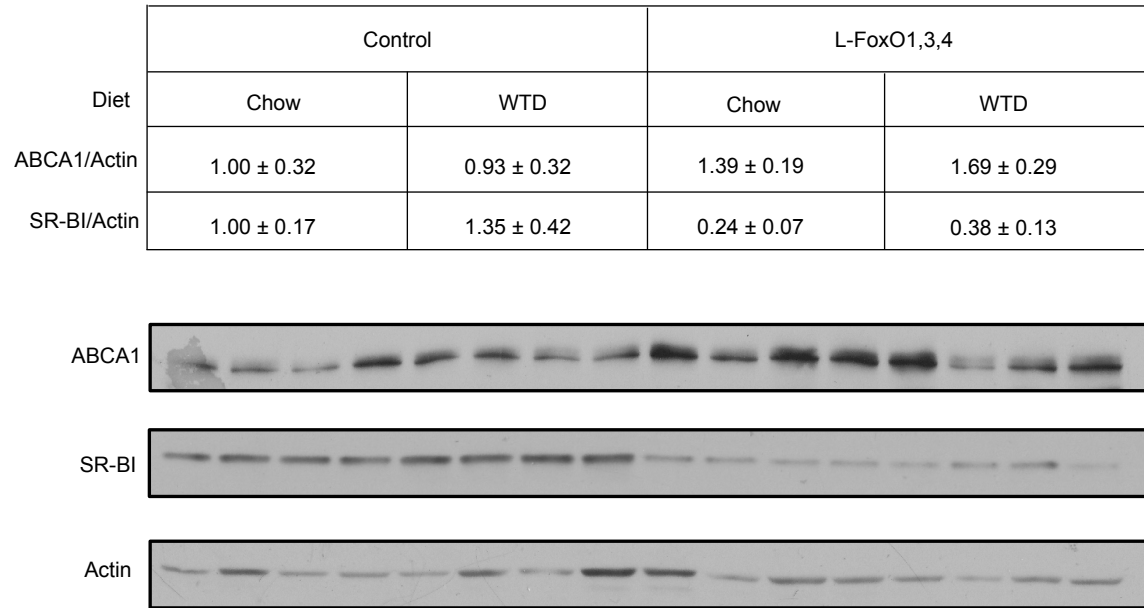|	Control		L-FoxO1,3,4	
Diet	Chow	WTD	Chow	WTD
ABCA1/Actin	1.00 ± 0.32	0.93 ± 0.32	1.39 ± 0.19	1.69 ± 0.29
SR-BI/Actin	1.00 ± 0.17	1.35 ± 0.42	0.24 ± 0.07	0.38 ± 0.13

Figure S2. Western Blot of Liver ABCA1 and SR-BI from Chow-Fed and WTD-Fed L-FoxO1,3,4 Mice. Related to Figure 2
Representative western blot of hepatic ABCA1 and SR-BI expression in both chow-fed and WTD-fed L-FoxO1,3,4 mice and littermate controls. ABCA1/Actin and SR-BI/Actin denote relative ABCA1 and SR-BI expression levels by densitometric scanning, respectively (n=4). ABCA1 antibody was commercially purchased from Novus (Novus – NB400-105). Data are presented as mean ± SEM.
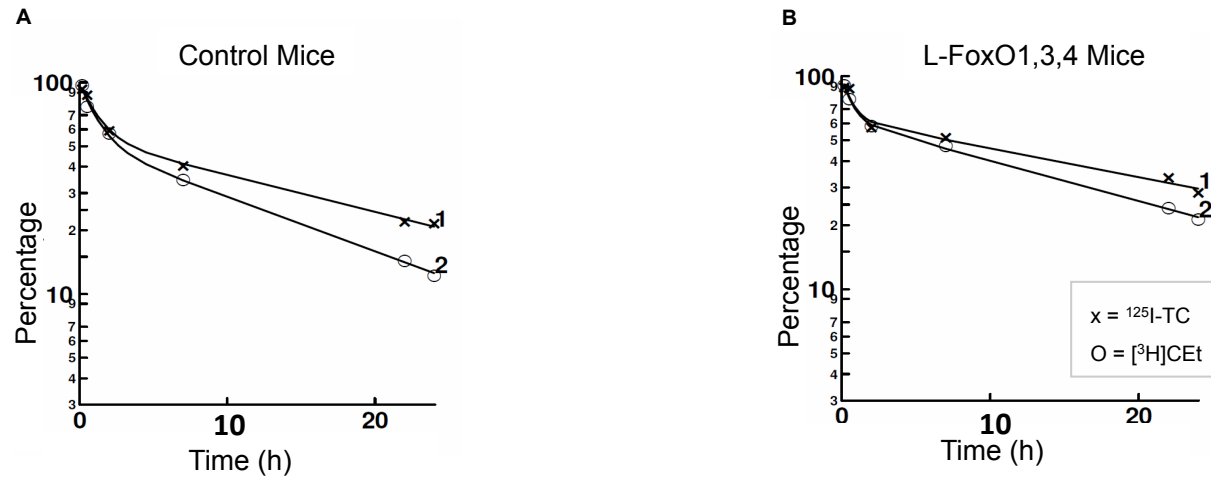
Supplemental Figure S3

Figure S3. Plasma Decay Kinetics of ^{125}I-TC-/[3H]CEt-WT-HDL in WTD-Fed L-FoxO1,3,4 Mice. Related to Figure 3

(A-B) ^{125}I-TC-/[3H]CEt-WT-HDL was injected intravenously in WTD-fed L-FoxO1,3,4 mice and littermate controls. Thereafter, during a 24-hr interval, periodic blood samples were harvested and plasma was analyzed for ^{125}I-TC (crosses) and [3H]CEt (circles). The y-axis represents the fraction of the tracer in plasma (%). Shown is a trace from a representative mouse from each genotype, with (A) control on the left and (B) L-FoxO1,3,4 on the right. The experiment was carried out in 6 control and 5 L-FoxO1,3,4 mice.

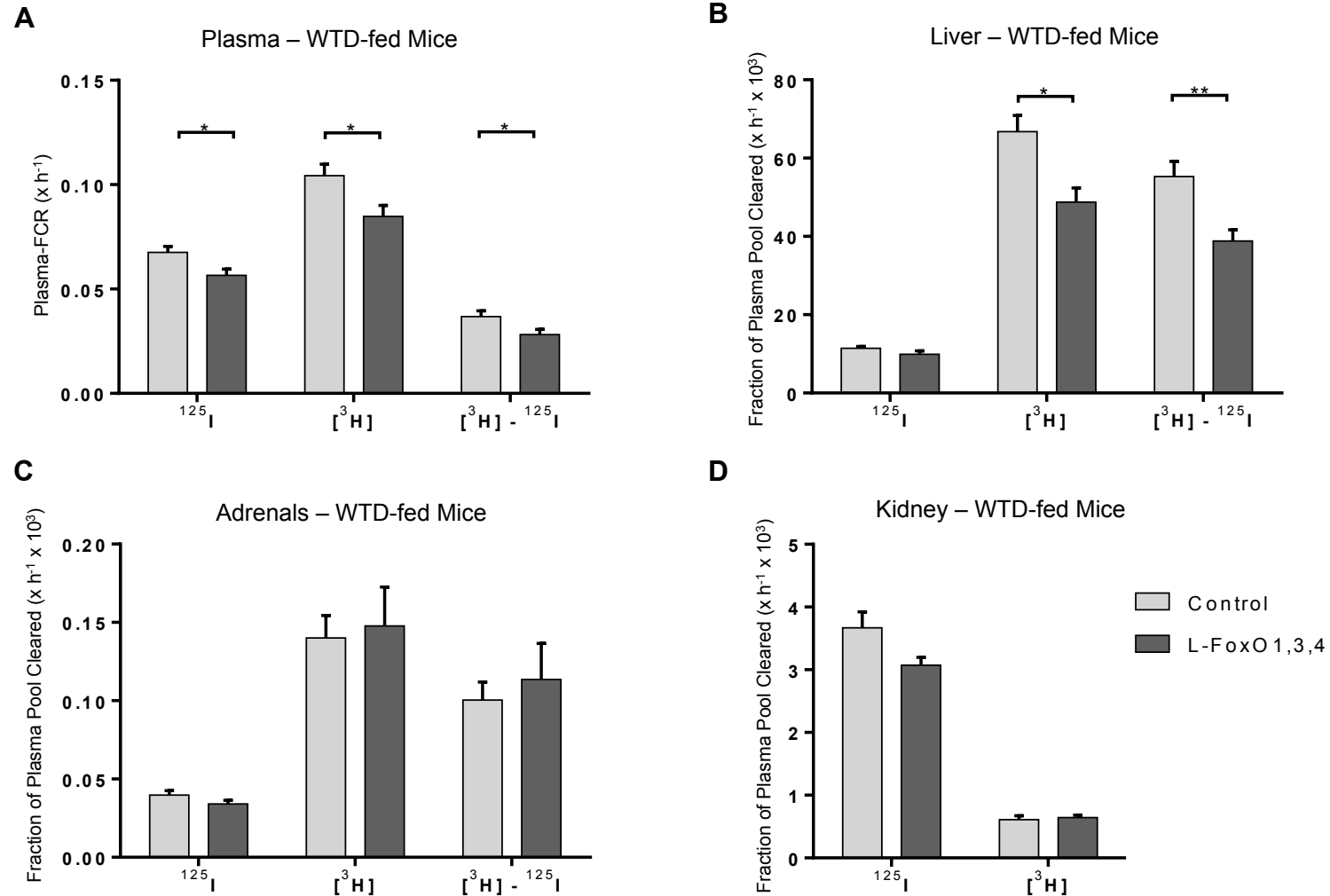**Figure S4. Plasma-FCRs and Tissue Tracer Uptake Rates for ¹²⁵I-TC-/[³H]CEt-WT-HDL in WTD-fed L-FoxO1,3,4 Mice. Related to Figure 4**

^{125}I-TC-/$[^3H]$CEt-WT-HDL was injected intravenously in WTD-fed L-FoxO1,3,4 mice and littermate controls. (A) During the subsequent 24-hr interval, blood was harvested periodically to determine the plasma decay of both tracers. ^{125}I-TC (^{125}I) and $[^3H]$CEt ($[^3H]$) were analyzed, and plasma-FCRs for ^{125}I-TC and $[^3H]$CEt were calculated. The difference in plasma-FCRs between $[^3H]$CEt and ^{125}I-TC was calculated. 24-hrs after tracer injection, the animals were euthanized, and tissues were analyzed for both tracers. (B) Liver, (C) adrenal and (D) kidney organ-FCRs for ^{125}I-TC (^{125}I), $[^3H]$CEt ($[^3H]$), and the difference in organ-FCRs between $[^3H]$CEt and ^{125}I-TC ($[^3H]$CEt - ^{125}I-TC) were calculated. All calculations were done as described in Materials and Methods. n = 6 control and n = 5 L-FoxO1,3,4 mice. An independent similar experiment with n=6 control mice and n=4 L-FoxO1,3,4 mice yielded qualitatively identical results as shown in the graphs. *p < 0.05, **p < 0.01, by Student's t-tests. Data are presented as mean ± SEM.
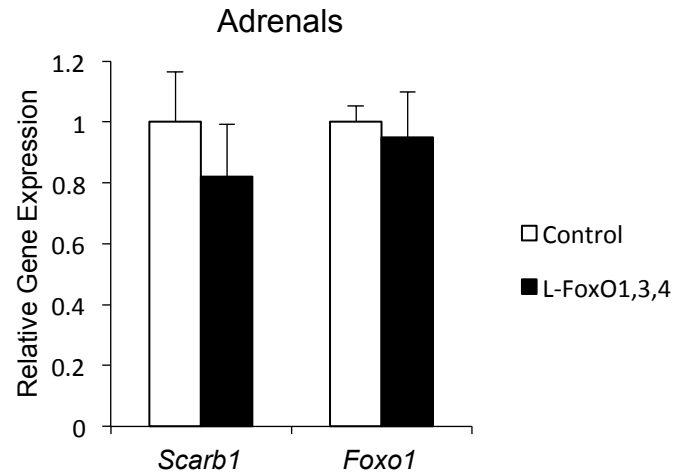
Supplemental Figure S5

Figure S5. Adrenal Gene Expression in Chow-Fed L-FoxO1,3,4 Mice. Related to Figure 4
Relative adrenal *Scarb1* and *Foxo1* gene expression by qPCR in chow-fed L-FoxO1,3,4 mice (n=3) and littermate controls (n=3). Data are presented as mean ± SEM.
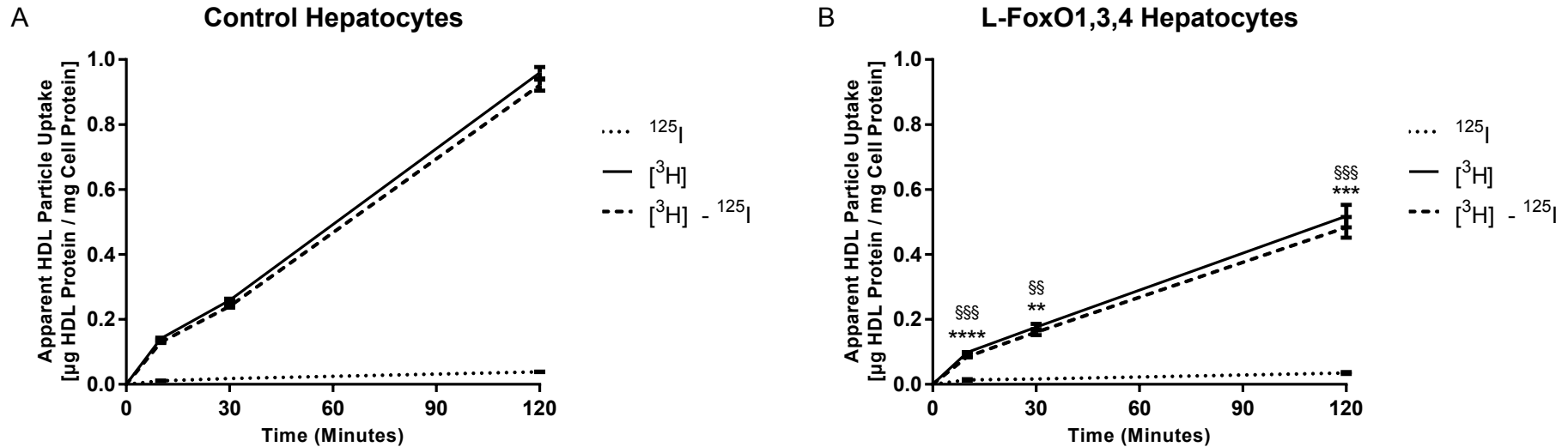
Supplemental Figure S6

A **Control Hepatocytes**

B **L-FoxO1,3,4 Hepatocytes**

Figure S6. Kinetics of Uptake of ^{125}I-TC-/[^{3}H]CEt-WT-HDL by Hepatocytes Isolated from Chow-Fed L-FoxO1,3,4 Mice. Related to Figure 5

(A-B) Hepatocytes from chow-fed L-FoxO1,3,4 mice and littermate controls were incubated (37°C, 10, 30 or 120 minutes) in medium containing ^{125}I-TC-/[^{3}H]CEt-WT-HDL (20 µg HDL protein/ml). Finally, cells were harvested, and apparent HDL particle uptake was analyzed as outlined in Materials and Methods. Values are means of (A) n = 3 (control) or of (B) n = 3 (L-FoxO1,3,4) independent determinations. Shown is a typical experiment. An independent similar experiment yielded qualitatively identical results. §§ $p < 0.01$, §§§ $p < 0.001$ comparing [^{3}H]CEt between L-FoxO1,3,4 and control hepatocytes; ** $p < 0.01$, *** $p < 0.001$, **** $p < 0.0001$ comparing [^{3}H]CEt - ^{125}I-TC between L-FoxO1,3,4 and control hepatocytes by Student's t-tests. Data are presented as mean ± SEM. Where no error bars are visible, the error was smaller than the symbol.

Supplemental Figure S7

A *Lipc* Expression
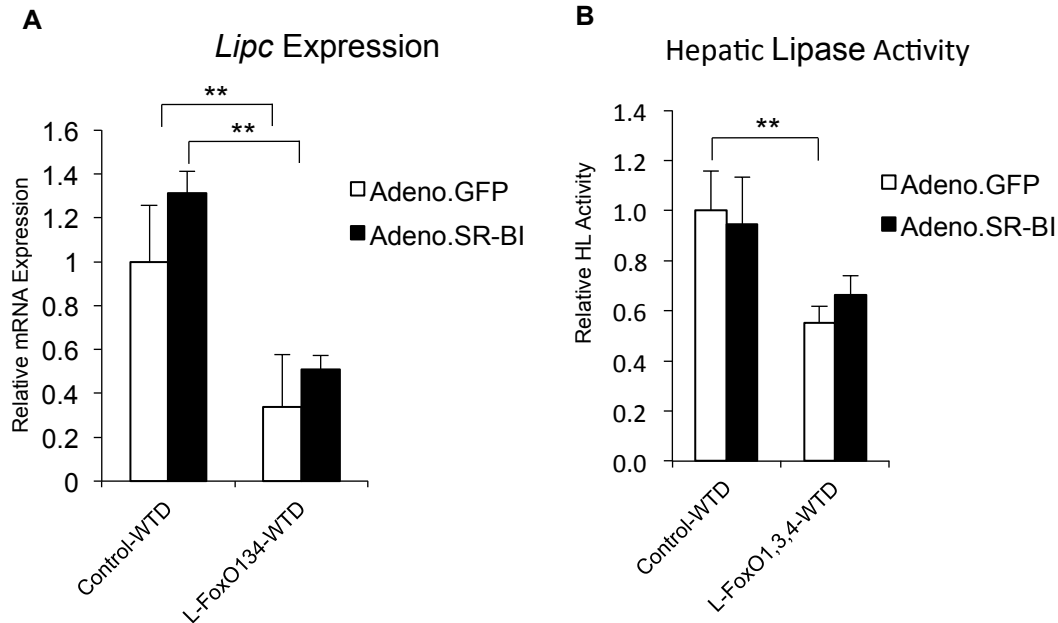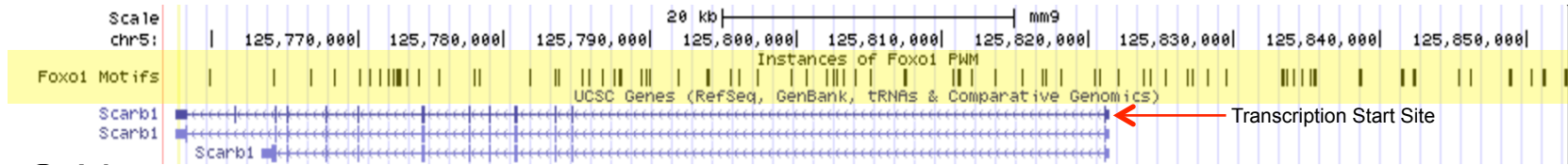
B Hepatic Lipase Activity

Figure S7. Effect of SR-BI Adenovirus on HL in WTD-fed L-FoxO1,3,4 Mice. Related to Figure 6 (A) Relative hepatic *Lipc* expression by qPCR in WTD-fed L-FoxO1,3,4 mice and littermate controls transduced with Adeno.SR-BI or control virus (Adeno.GFP). (n=3-4). **p<0.01 by two-way ANOVA. (B) Relative Plasma hepatic lipase activity in same mice as (A). **p<0.01 by two-way ANOVA.

Supplemental Figure S8

A

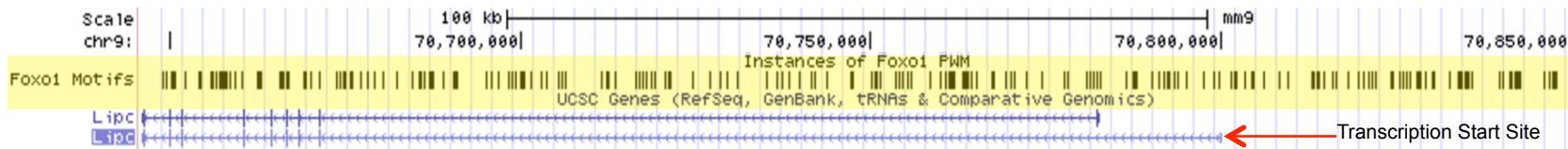| Gene Name	Motifs within gene sequence	Motifs from transcription start site to 5kb upstream	Motifs from 5kb-20kb upstream	Motifs from 20kb-50kb upstream	Total Motifs from end of gene to 50kb upstream
Scarb1	59	4	16	31	=110
Lipc	174	7	14	42	=237

B *Scarb1*

C *Lipc*

Figure S8. Potential FoxO Binding Site Analysis of *Scarb1* and *Lipc* Using HOMER Motif Discovery Algorithm.
(A) Summary of potential FoxO binding motifs near *Scarb1* and *Lipc*. The entire sequences for mouse *Scarb1* and *Lipc*, along with 50kb of sequence upstream of their respective transcription start sites were taken from the UCSC Genome Browser (https://genome.ucsc.edu). The sequences were analyzed by the HOMER algorithm software, which provided the coordinates of all the potential FoxO binding motifs within the selected regions. Values are grouped by motifs within the gene sequence, motifs from the transcription start site to 5kb upstream of start site, 5kb-20kb upstream of start site, 20kb-50kb upstream of start site, and total number of motifs.
(B-C) Schematics from the UCSC Genome Browser highlighting positions of all motifs in selected region for (B) *Scarb1* and (C) *Lipc*. Highlighted in yellow are the relative coordinates of all potential FoxO binding motifs found though HOMER. Each motif is represented as a vertical line ("|"). Transcription start sites are indicated by the red arrow (both genes are transcribed in the reverse direction).
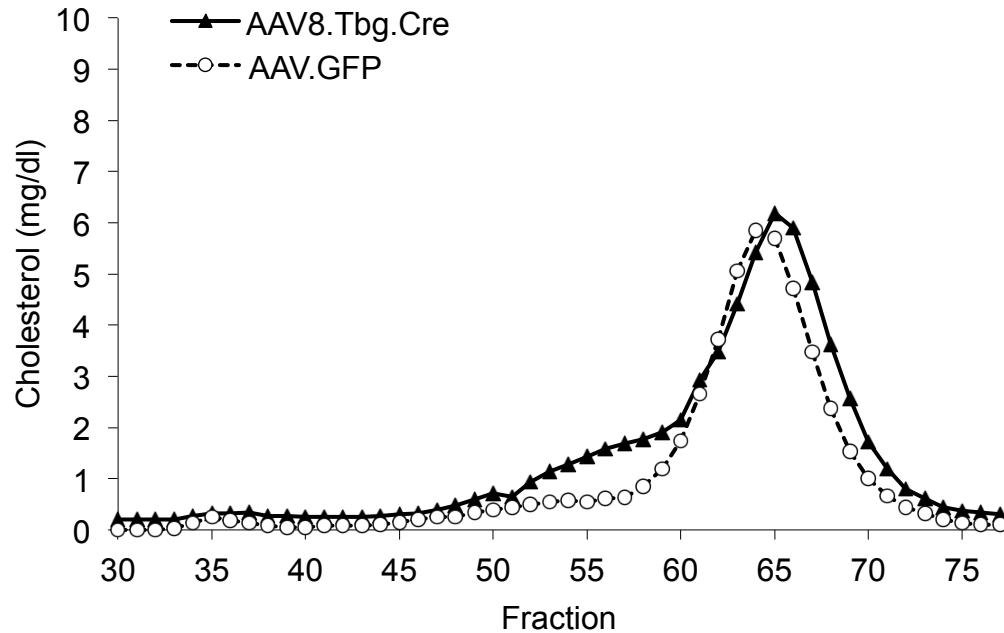
Supplemental Figure S9

Figure S9. Cholesterol Levels in Plasma Fractionated by FPLC in Chow-fed Hepatic FoxO Floxed Mice Transduced with Liver Specific Adeno-Associated Virus Expressing Cre. **Related to Figure 7**

Plasma was collected 2 weeks after virus transduction and fractionated by FPLC in chow-fed, adult control mice containing all three FoxO alleles floxed (*Foxo1flox/flox*, *Foxo3flox/flox*, and *Foxo4flox/Y*), and transduced with liver specific adeno-associated virus expressing either Cre (AAV8.Tbg.Cre) or control virus (AAV.GFP).

Supplemental Figure S10
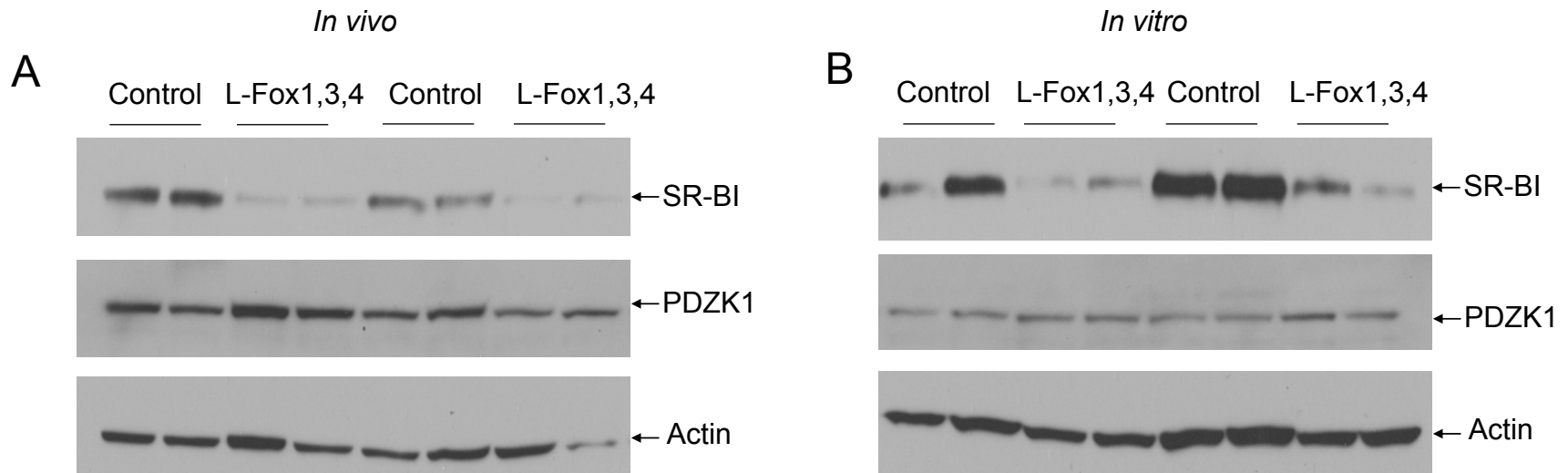
Figure S10. Western Blot of Liver PDZK1 from WTD-Fed L-FoxO1,3,4 Mice and Hepatocytes Isolated from L-FoxO1,3,4 mice. Related to Figure 7

(A-B) Representative western blot of hepatic PDZK1 expression from (A) WTD-fed L-FoxO1,3,4 mice and littermate controls *in vivo*, or (B) hepatocytes isolated from chow-fed L-FoxO1,3,4 mice and littermate controls *in vitro*. PDZK1 antibody was commercially purchased from Novus (Novus – NB400-149).

Supplemental Figure Legends

Figure S1. Western Blot of Total Plasma apoA-I. Related to Figure 1
(A-B) Plasma was collected from (A) chow-fed and (B) WTD-fed L-FoxO1,3,4 mice and littermate controls. Plasma was diluted by 1:200 with PBS, from which 20µl from each sample were run on a 4%-15% Tris-HCL gradient gel and blotted for apoA-I. Numbers denote relative apoA-I expression levels by densitometric scanning (n=4-7). Values are presented as mean ± SEM. Shown is a typical experiment. Independent experiments yielded qualitatively identical results.

Figure S2. Western Blot of Liver ABCA1 and SR-BI from Chow-Fed and WTD-Fed L-FoxO1,3,4 Mice. Related to Figure 2
Representative western blot of hepatic ABCA1 and SR-BI expression in both chow-fed and WTD-fed L-FoxO1,3,4 mice and littermate controls. ABCA1/Actin and SR-BI/Actin denote relative ABCA1 and SR-BI expression levels by densitometric scanning, respectively (n=4). ABCA1 antibody was commercially purchased from Novus (Novus – NB400-105). Data are presented as mean ± SEM.

Figure S3. Plasma Decay Kinetics of ^{125}I-TC-/[^{3}H]CEt-WT-HDL in WTD-Fed L-FoxO1,3,4 Mice. Related to Figure 3
(A-B) ^{125}I-TC-/[^{3}H]CEt-WT-HDL was injected intravenously in WTD-fed L-FoxO1,3,4 mice and littermate controls. Thereafter, during a 24-hr interval, periodic blood samples were harvested and plasma was analyzed for ^{125}I-TC (crosses) and [^{3}H]CEt (circles). The y-axis represents the fraction of the tracer in plasma (%). Shown is a trace from a representative mouse from each genotype, with (A) control on the left and (B) L-FoxO1,3,4 on the right. The experiment was carried out in 6 control and 5 L-FoxO1,3,4 mice.

Figure S4. Plasma-FCRs and Tissue Tracer Uptake Rates for ^{125}I-TC-/[^{3}H]CEt-WT-HDL in WTD-Fed L-FoxO1,3,4 Mice. Related to Figure 4
^{125}I-TC-/[^{3}H]CEt-WT-HDL was injected intravenously in WTD-fed L-FoxO1,3,4 mice and littermate controls. (A) During the subsequent 24-hr interval, blood was harvested periodically to determine the plasma decay of both tracers. ^{125}I-TC (^{125}I) and [^{3}H]CEt ([^{3}H]) were analyzed, and plasma-FCRs for ^{125}I-TC and [^{3}H]CEt were calculated. The difference in plasma-FCRs between [^{3}H]CEt and ^{125}I-TC was calculated. 24-hrs after tracer injection, the animals were euthanized, and tissues were analyzed for both tracers. (B) Liver, (C) adrenal and (D) kidney organ-FCRs for ^{125}I-TC (^{125}I), [^{3}H]CEt ([^{3}H]), and the difference in organ-FCRs between [^{3}H]CEt and ^{125}I-TC ([^{3}H]CEt - ^{125}I-TC) were calculated. All calculations were done as described in Materials and Methods. n = 6 control and n = 5 L-FoxO1,3,4 mice. An independent similar experiment with n=5 control mice and n=4 L-FoxO1,3,4 mice yielded qualitatively identical results as shown in the graphs. *p < 0.05, **p < 0.01, by Student's t-tests. Data are presented as mean ± SEM.

Figure S5. Adrenal Gene Expression in Chow-Fed L-FoxO1,3,4 Mice. Related to Figure 4
Relative adrenal *Scarb1* and *Foxo1* gene expression by qPCR in chow-fed L-FoxO1,3,4 mice (n=3) and littermate controls (n=3). Data are presented as mean ± SEM.

Figure S6. Kinetics of Uptake of ^{125}I-TC-/[^{3}H]CEt-WT-HDL by Hepatocytes Isolated from Chow-Fed L-FoxO1,3,4 Mice. Related to Figure 5
(A-B) Hepatocytes from chow-fed L-FoxO1,3,4 mice and littermate controls were incubated (37°C, 10, 30 or 120 minutes) in medium containing ^{125}I-TC-/[^{3}H]CEt-WT-HDL (20 µg HDL protein/ml). Finally, cells were harvested, and apparent HDL particle uptake was analyzed as outlined in Materials and Methods. Values are means of (A) n = 3 (control) or of (B) n = 3 (L-FoxO1,3,4) independent determinations. Shown is a typical experiment. An independent similar experiment yielded qualitatively identical results. §§ p < 0.01, §§§ p < 0.001 comparing [^{3}H]CEt between L-FoxO1,3,4 and control hepatocytes; ** p < 0.01, *** p < 0.001, **** p < 0.0001 comparing [^{3}H]CEt - ^{125}I-TC between L-FoxO1,3,4 and control hepatocytes by Student's t-tests. Data are presented as mean ± SEM. Where no error bars are visible, the error was smaller than the symbol.

Figure S7. Effect of SR-BI Adenovirus on HL in WTD-fed L-FoxO1,3,4 Mice. Related to Figure 6
(A) Relative hepatic *Lipc* expression by qPCR in WTD-fed L-FoxO1,3,4 mice and littermate controls transduced with Adeno.SR-BI or control virus (Adeno.GFP). (n=3-4). **p<0.01 by two-way ANOVA. (B) Relative Plasma hepatic lipase activity in same mice as (A). **p<0.01 by two-way ANOVA.

Figure S8. Potential FoxO Binding Site Analysis of *Scarb1* and *Lipc* Using HOMER Motif Discovery Algorithm.
(A) Summary of potential FoxO binding motifs near *Scarb1* and *Lipc*. The entire sequences for mouse *Scarb1* and *Lipc*, along with 50kb of sequence upstream of their respective transcription start sites were taken from the UCSC Genome Browser (https://genome.ucsc.edu). The sequences were analyzed by the HOMER algorithm software, which provided the coordinates of all the potential FoxO binding motifs within the selected regions. Values are grouped by motifs within the gene sequence, motifs from the transcription start site to 5kb upstream of start site, 5kb-20kb upstream of start site, 20kb-50kb upstream of start site, and total number of motifs.
(B-C) Schematics from the UCSC Genome Browser highlighting positions of all motifs in selected region for (B) *Scarb1* and (C) *Lipc*. Highlighted in yellow are the relative coordinates of all potential FoxO binding motifs found though HOMER. Each motif is represented as a vertical line ("|"). Transcription start sites are indicated by the red arrow (both genes are transcribed in the reverse direction).

Figure S9. Cholesterol Levels in Plasma Fractionated by FPLC in Chow-fed Hepatic FoxO Floxed Mice Transduced with Liver Specific Adeno-Associated Virus Expressing Cre. **Related to Figure 7**
Plasma was collected 2 weeks after virus transduction and fractionated by FPLC in chow-fed, adult control mice containing all three FoxO alleles floxed (*Foxo1$^{flox/flox}$*, *Foxo3$^{flox/flox}$*, and *Foxo4$^{flox/Y}$*), and transduced with liver specific adeno-associated virus expressing either Cre (AAV8.Tbg.Cre) or control virus (AAV.GFP).

Figure S10. Western Blot of Liver PDZK1 from WTD-Fed L-FoxO1,3,4 Mice and Hepatocytes Isolated from L-FoxO1,3,4 mice. Related to Figure 7
(A-B) Representative western blot of hepatic PDZK1 expression from (A) WTD-fed L-FoxO1,3,4 mice and littermate controls *in vivo*, or (B) hepatocytes isolated from chow-fed L-FoxO1,3,4 mice and littermate controls *in vitro*. PDZK1 antibody was commercially purchased from Novus (Novus – NB400-149).

Table S1. L-FoxO1,3,4 Microarray From Liver Tissues. Microarrays were performed from liver tissues of chow-fed L-FoxO1,3,4 mice and littermate controls (Haeusler et al., 2014).

Gene	Control	L-FoxO1,3,4	*P* value
Scarb1	**1**	**0.727**	**0.043**
Lipc	**1**	**0.364**	**0.00091**
Abca1	1	1.132	0.27
Apoa1	1	0.950	0.17
Apoa2	1	0.96	0.56
Apoc3	1	0.86	0.28
Apoe	1	0.951	0.25
Lcat	1	1.021	0.86
Srebp2	1	0.80	0.47
Hmgcr	1	0.473	0.22
Pltp	1	1.89	0.11
Abcg5	1	0.928	0.76
Abcg8	1	0.825	0.532

Supplemental Experimental Procedures
Primer Sequences. Primer sequences for genes that were measured via qPCR. For liver and adrenal tissues, genes were normalized to *36b4*. For primary hepatocytes, genes were normalized to *B2m*.

Gene	Direction	Sequence (5'-3')
36b4	Forward	AGATGCAGCAGATCCGCAT
36b4	Reverse	GTTCTTGCCCATCAGCACC
B2m	Forward	CTGGTGCTTGTCTCACTGAC
B2m	Reverse	GTTCAGTATGTTCGGCTTCC
Abca1	Forward	GGTTTGGAGATGGTTATACAATAGTTGT
Abca1	Reverse	CCCGGAAACGCAAGTCC
Abcg5	Forward	TGGATCCAACACCTCTATGCTAAA
Abcg5	Reverse	GGCAGGTTTTCTCGATGAACTG
Abcg8	Forward	GTAGCTGATGCCGATGACAA
Abcg8	Reverse	GGGGCTGATGCAGATTCA
Apoa1	Forward	TGTGTATGTGGATGCGGTCA
Apoa1	Reverse	ATCCCAGAAGTCCCGAGTCA
Apoc3	Forward	GCATCTGCCCGAGCTGAAGAG
Apoc3	Reverse	CTGAAGTGATTGTCCATCCAGC
Apoe	Forward	CCGGTGCTGTTGGTCACATTGCTGACAGGAT
Apoe	Reverse	GTTCTTGTGTGACTTGGGAGCTCTGCAGCT
Foxo1	Forward	TCCAGTTCCTTCATTCTGCACT
Foxo1	Reverse	GCGTGCCCTACTTCAAGGATAA
G6pc	Forward	GTCTGGATTCTACCTGCTAC
G6pc	Reverse	AAAGACTTCTTGTGTGTCTGTC
Gck	Forward	CTGTTAGCAGGATGGCAGCTT
Gck	Reverse	TTTCCTGGAGAGATGCTGTGG
Hmgcr	Forward	CTTGTGGAATGCCTTGTGATTG
Hmgcr	Reverse	AGCCGAAGCAGCACATGAT
Lcat	Forward	GCTGGCCTGGTAGAGGAGATG
Lcat	Reverse	CCAAGGCTATGCCCAATGA
Lipc	Forward	GACGGGAAGAACAAGATTGG
lipc	Reverse	GGCATCATCAGGAGAAAGG
Pltp	Forward	TGGGACGGTGTTGCTCAA
Pltp	Reverse	CCCACGAGATCATCCACAGA
Scarb1	Forward	GGCTGCTGTTTGCTGCG
Scarb1	Reverse	GCTGCTTGATGAGGGAGGG
Srebp2	Forward	GATGATCACCCCGACGTTCAG
Srebp2	Reverse	GTACCGTCTGCACCTGCTGCT